I. ON THE APPLICATION OF A LASER TO HIGH SPEED PHOTOGRAPHY

II. TORSIONAL MAGNETOELASTIC WAVES IN A CIRCULAR CYLINDER

Thesis by
M. E. Fourney

In Partial Fulfillment of the Requirements
For the Degree of
Doctor of Philosophy

California Institute of Technology
Pasadena, California

1963

ACKNOWLEDGEMENT

The author would like to express his thanks for the guidance provided by Professor A. T. Ellis throughout the course of this investigation. Also he would like to take this opportunity to thank Professor E. E. Sechler for the guidance and encouragement received throughout the entire graduate program, both of a technical and personal nature.

The efficient, complete, and friendly library services provided by Mrs. Katherine McColgan have been invaluable. Special thanks are due to Mr. Carl Eastvedt for his patience and cheerfulness while spending many long hours with the author in the processing of film, which in many cases was found to be completely blank. Also the ungrudging and efficient services of Mrs. Verena Scheidegger are acknowledged for typing this thesis as well as other associated papers.

Finally the support of the Office of Naval Research, Department of the Navy, U.S.A., is gratefully acknowledged.

ABSTRACT

The first part of this thesis deals with the application of a ruby laser to high speed photography. The light that is emitted from a ruby laser is monochromatic, collimated, coherent, linearly polarized, and highly intense. It has been demonstrated that these properties make the laser a very useful tool for research in areas involving photographic techniques.

A method has been devised by which the output of the laser is controlled and is emitted in the form of a series of light pulses. The rate at which these pulses are generated can be controlled and repetition rates of over 1.6 Mc/sec have been achieved. The 30 nsec duration of an individual pulse represents the exposure time for a high speed laser camera which has been developed. Pictures have been taken at rates of over 1.2 million frames per second. This exposure time represents a reduction of an order of magnitude over that previously possible, with an increase of three orders of magnitude in intensity. In applications where a particular characteristic of the laser light is required, such as the monochromatic nature desired in photoelasticity, this improvement of four orders of magnitude is further increased.

When a series of light pulses is generated in the manner described above it is found that the amplitude of the pulse train becomes stable above a certain critical frequency. This critical frequency is determined to be a function of the laser cavity length. The amplitude of the stabilized pulse train is a function of the repetition rate and the cavity length. The nature of this variation is established and a mechanistic explanation of the phenomena involved is presented.

TABLE OF CONTENTS

Part I

LIST OF SYMBOLS

A_{nm} ~ spontaneous transition probability between state n and m

B_{nm} ~ stimulated transition probability

c ~ velocity of light

E_i ~ energy of atom in i^{th} state

F ~ net factor by which radiation is changed in one complete passage in laser cavity

g_n ~ multiplicity of n level

h ~ Planck's constant

I_o ~ intensity of radiation

I_ν ~ intensity of radiation of frequency ν

k ~ Boltzmann's constant

k_ν ~ absorption coefficient for radiation of frequency ν

L ~ length of active material in laser cavity

N_j ~ number of atoms in j^{th} state

N_o ~ total number of atoms in ensemble

p ~ power emitted from laser

P ~ peak power output

P_{nm} ~ total transition probability between state n and m

r ~ geometric mean of reflection coefficients

r_i ~ reflection coefficient of i^{th} end of laser cavity

R ~ repetition rate

s ~ separation of external mirror

S_{ij} ~ spontaneous non-radiation transition probability between state i and j

t ~ transmission coefficient of partial reflector

T ~ absolute temperature

u ~ radiation density

u_ν ~ radiation density of frequency ν

W_{ij} ~ spontaneous transition probability between state i and j

α ~ amplification coefficient

α_m ~ maximum amplification coefficient

γ ~ loss coefficient

η ~ index of refraction

λ ~ wavelength

ν ~ frequency of radiation

ν_{nm} ~ frequency of radiation corresponding to transition between state n and m

σ_{ij} ~ absorption cross section for transition between state i and j

INTRODUCTION

The field of lasers is a new and rapidly expanding one. The laser was first conceived in a paper by A. L. Schawlow and C. H. Townes[1] which appeared in 1958. In July 1960, T. H. Maiman[2] demonstrated the first operational laser. In less than three years the laser has become one of the major items of research in this country. Although it is originally an outgrowth of research in microwaves, applications have been proposed in most of the major fields in science. Due to this great variety of applications the primary research interest has been produced in the industries. Consequently it has been an extremely competitive field of research.

The literature on laser research has grown in the past year and a half to extreme proportions. Prior to this very little was published, due primarily to the competitive nature of the research involved. Until very recently the results of this research were widely scattered in a variety of journals. A start has been made to combine this into proceedings of symposiums [3, 4] and textbooks on the subject.[5] However, the literature is still mainly in the form of articles, therefore it is quite difficult to give any semblance of a literature survey on the subject. The best that might be done is to refer the interested reader to special issues in the journals on the subject [6, 7] or special lists of references.[8]

The primary purpose for which this research was undertaken was to fulfill the need for a light source to be used in high speed dynamic photoelasticity. For such experiments the ideal light source should possess the following properties: (a) monochromaticity, (b) high intensity, and (c) ability to be converted efficiently into a collimated beam. In addition, linearly polarized light is required; if the intensity is sufficient this is achieved by a polarizing element.

The light from a laser, which is an acronym for light amplification by the stimulated emission of radiation, has the following properties.

(a) Monochromaticity; the light emitted from a laser is monochromatic to within less than 0.1 A^{o} in bandwidth. In the area of photoelasticity as well as several others it is essential to have light which possesses this property. Before the advent of the laser, in practice it was possible to achieve nearly monochromatic light (within 100 A^{o} bandwidth) only for relatively long exposure times (several μsec) in high speed photography. For higher speeds the monochromatic property was of necessity sacrificed to achieve sufficient intensity.

(b) High intensity; the laser beam at present may be focused to yield intensities of over 10^{12} watts/cm^2. This is about 100 million times the power density at the surface of the sun. But of more importance is the fact that this radiation falls within a spectral interval of the order of 0.1 A^{o} wide. The previous sources of radiation for high speed photography were Xenon flashtubes which produced only about 0.016 watts/cm^2 in a 0.1 A^{o} interval.[5]

(c) The output of the laser beam is a well defined collimated beam of light. The angular divergence of this beam is less than 1^{o}. Under carefully controlled conditions a beam width of about 1 milliradian divergence can be achieved.

(d) The output of a ruby laser is linearly polarized when the optic axis of the ruby is at 60 or 90^{o} to the rod axis. Nelson and Collins[9] have found that the light is 100 percent linearly polarized with the electric vector perpendicular to the plane containing the optic axis.

(e) The light is both time-wise and space-wise coherent. This property is not of great importance in photographic applications, however, it is in other areas.

Therefore it may easily be seen that the laser light has all the ideal characteristics desired.

The purpose of this research was to devise a method by which the laser could be used in the area of high speed photography. In pro-

viding this tool for research it was felt that the applications which were used to prove its value need not necessarily be those which were responsible for its conception. Therefore it will be noted in section D that the primary field of applications have to do with cavitation and fluid flow. Although several other areas of applications are demonstrated or proposed, no conscientious attempt has been made to define even the major areas of the application of a laser to high speed photographs.

As the primary objective of this investigation was experimental in nature much of the material presented in section A on the fundamentals of a laser may be found either in general textbooks on the subject of quantum mechanics[10, 11] or in survey articles on the subject such as one by Levine[12]. Likewise some of the articles by Maiman[13, 14] and McClung and Hellwarth[15] were quite helpful in providing a theoretical background for this section.

SECTION A: FUNDAMENTALS OF A THREE LEVEL LASER

I. Emission, Absorption and Amplification of Radiation

Atomic systems such as ions, atoms and molecules possess certain stationary states each of which corresponds to definite values of energy. These states are characterized by numbers called quantum numbers. Transitions between these states may occur by the transfer of energy by the processes of emission or absorption of radiation, by transfer to another system, or by dissipation of energy by processes such as molecular vibration, etc. If the transfer of energy is by radiation the frequency of this radiation, which may be either absorbed or emitted by the system, is given by Bohr's frequency relation:

$$h\nu = E_2 - E_1 \qquad (1)$$

where E_1 and E_2 are the energies of the states between which the transition takes place, h is Planck's constant and ν the frequency of the radiation.

The lowest value of energy of a system corresponds to the ground state or level. It is necessary here to differentiate between level and state. Specific values of energy are denoted as a level, however, a system may have more than one state corresponding to a specific energy or level. In the latter case the level is called degenerate and the number of states in the level is known as the multiplicity of the level.

There are three basic methods by which a transition may take place between two levels, these are shown in Fig. 1. The state of the ion is represented by a black dot, the radiation by an arrow. In absorption the ion is initially in the ground state and is excited by a photon of frequency ν_{12}. Upon absorption of this photon the ion is raised to a level corresponding to E_2. Likewise the processes of spontaneous and stimulated emission are shown.

The probability that a system in level n will spontaneously change to a lower level m within a unit time is called the

spontaneous transition probability* and is denoted by A_{nm}. The total probability that this system will change from a higher level n to a lower one m is:

$$P_{nm} = A_{nm} + u_\nu B_{nm} \qquad (2)$$

where u_ν is the radiation density at the frequency that corresponds to the energy difference of the levels. B_{nm} is the stimulated transition probability. The probability of the system changing from a lower level m to a higher one n is:

$$P_{mn} = u_\nu B_{mn} \qquad (3)$$

It is evident therefore that radiation emitted by an atomic system in the presence of external radiation consists of two parts; the first whose intensity is proportional to A_{nm} and is independent of the external radiation, the second, or stimulated part, whose intensity is proportional to the product of the external radiation density u_ν and its transition probability B_{nm}.

To conclude this brief discussion of the transition between energy levels it is noted that these transition probability coefficients, or Einstein coefficients, are related in the following manner:

$$B_{nm} = B_{mn} \quad , \quad A_{nm} = \frac{8\pi h\nu^3}{c^3} B_{nm} \qquad (4)$$

where c is the velocity of light. When the levels are degenerate and the index of refraction η differs appreciably from unity these relations take the form:

$$g_n B_{nm} = g_m B_{mn} \quad , \quad A_{nm} = \frac{8\pi h\nu^3\eta^3}{c^3} B_{nm} \qquad (5)$$

---

*Lengyel of reference (5) points out that these quantities are strictly speaking rates, not probabilities and that their dimensions are that of reciprocal time.

where g_n and g_m are the multiplicities of the levels.

The distribution of the atoms in each of these states is governed by Boltzmann's law. For a large number of atoms N_o in thermal equilibrium at absolute temperature T the number in the j^{th} state is given by:

$$N_j' = \frac{N_o \exp(-E_j/kT)}{\sum_i \exp(-E_i/kT)} \qquad (6)$$

where E_j is the energy of the j^{th} state. Since the energy for all states of a given level is constant, by equation (6) each state is equally populated and total number of atoms in level n is $N_n = g_n N_n'$. Thermal equilibrium requires the number of atoms in the higher energy state to be less than that of the lower one. At normal temperatures relatively few atoms will be in an excited state due to the size of the exponent in equation (6).*

Consider the case where an ensemble of atoms, not necessarily in thermal equilibrium, has N_n atoms per unit volume in the n^{th} state. Radiation of frequency ν_{nm} is incident upon this ensemble, where $n > m$. The number of downward transitions from level n to level m is given by equation (2) as $(A_{nm} + uB_{nm})N_n$ per unit time. Likewise the number of upward transitions will be $uB_{mn}N_m$. Hence if $N_n < N_m$ the incident beam suffers a net loss of $(N_m - N_n)uB_{nm}$ quanta per unit time. This is schematically shown in Fig. 2, (note that the net change is proportional to the radiation density). The $A_{nm}N_n$ quanta, which are radiated spontaneously, will appear as scattered radiation. A material which has a relatively more populated lower state than upper state causes a decrease in the intensity of the incident beam and is said to have a positive absorption coefficient.

Population inversion in a material is defined as the condition that exists when the number of atoms in the excited state N_n

* The first excited state for most systems is at least 2×10^{-2} ergs above ground state and at $500^{\circ}K$, the product kT is 0.07×10^{-12} ergs.

exceeds those in N_m even though $n > m$. This is not a condition of thermal equilibrium as is indicated by equation (6). Referring once more to Fig. 2 it is seen that the net gain of intensity when population inversion has been achieved is $(N_n - N_m)uB_{nm}$. The incident beam of frequency ν_{nm} has thus been amplified by this amount, and the scattered spontaneous radiation thus appears as amplifier noise. This condition of population inversion thus requires the material to be in thermal non-equilibrium. The manner in which this is achieved will be discussed later.

In later sections it will be necessary to have a quantitative understanding of this amplification process, hence the quantitative process of absorption must be considered. In order to do this it is necessary for the moment to sacrifice the mathematical idealization concerning the infinite sharpness of the energy levels and spectra lines. It is observed, when radiation of a constant intensity I_o but variable frequency is incident upon an absorbent medium, that at a depth within the medium the intensity of the radiation is given by:

$$I_\nu = I_o e^{-k_\nu x} \qquad (7)$$

By varying the frequency and measuring the intensity, an absorption coefficient curve of the type shown in Fig. 3 is obtained. This general shape is characteristic and will play an important part in a following section on the threshold conditions. As indicated previously when population inversion has been achieved the absorption coefficient as defined here becomes negative and hence will be called the amplification coefficient.

II. General Description of the Operation of a Ruby Laser

The ruby laser falls into a general class called a three-level laser. Figure 4 shows the generalized energy levels for a three level fluorescent solid. As stated previously, by definition, a laser implies an amplicication of light of one particular frequency. The basic problem which must be overcome is that of achieving a suffi-

cient degree of negative absorption to allow laser action to take place. To facilitate discussion of how this process is achieved, reference will be made to Fig. 4. The levels on this diagram are numbered and schematically characterized; that is, 1 denotes the ground level, 2 a long lived excited state from which the stimulated emission takes place, and 3 a broad pumping band in which the atoms have a short lifetime and which is connected to state 2 via a spontaneous non-radiative transition. In the three-level laser it is the combination of this broad pumping band connected to the long lived excited state which makes population inversion possible.

In Fig. 4 the transitions are labeled according to type; that is, stimulated transitions are indicated by W, spontaneous radiative ones by A, and spontaneous non-radiative one by S. Hence when the pumping radiation is supplied to a three level laser, the ions originally in the ground state are raised to level 3 via the process labeled W_{13}. The lifetime in this level is very short, in the submicrosecond range, hence ions leave this state and return to the ground state by both stimulated and spontaneous transitions, however, most of the absorbed energy is transferred by a rapid non-radiative process to the long lived level 2. The lifetime in this state for ruby is of the order of 2 or 3 msec.[14] Here they tend to accumulate if sufficient energy is supplied and quickly achieve a population inversion. Hence the first group of spontaneous transitions from level 2 to the ground state will stimulate transition from this level which in turn will result in a cascading process if the laser cavity is properly shaped. Due to the nature of stimulated emission the output of the laser will be coherent and monochromatic. Due to the crystalline structure of the ruby the radiation will also be linearly polarized.

III. Threshold Conditions

In order that lasing action may take place two conditions must be fulfilled; (a) a population inversion must be attained, (b) a threshold condition must be met. The population inversion has been

discussed. The study of the threshold condition may most easily be approached by setting up the condition necessary for oscillations of light to grow within a laser cavity. A schematic diagram of a laser cavity is shown in Fig. 5. The cavity consists of the active ruby material and a reflector at each end. One reflector is as far as possible total reflective, the other partially reflective to permit a means of escape for the laser output. If the losses at these reflectors are assumed negligible the total loss within the cavity is due to the amount of radiation transmitted through these reflectors and the losses within the active material. If the reflective coefficients of the two mirrors are denoted by r_1 and r_2, then at each reflection a fraction $1-r$ of the radiation is returned to the cavity. Radiation starting at one point in the cavity must make two reflections before it returns to this same point traveling in the same direction. If population inversion has been achieved the intensity of light traveling in the cavity is increased according to the equation

$$I = I_0 e^{\alpha x} \qquad (8)$$

where α, the amplification coefficient, is the negative of the absorption coefficient of equation (7). In each complete passage through the material the intensity grows by the factor $e^{2\alpha L}$, where L is the length of the cavity. Now if the oscillation is to be sustained the gain of the radiation must exceed the losses. The net factor by which the radiation will have changed is given by

$$F = r_1 r_2 e^{2\alpha L} \qquad (9)$$

For convenience, r, the geometric mean of r_1 and r_2 is introduced and a loss coefficient

$$\gamma = -\log_e r \qquad (10)$$

is defined. Therefore the gain in one complete pass is given by

$$F = \exp 2(\alpha L - \gamma) \qquad (11)$$

Oscillations will build up if $F \geq 1$ and will decay if $F < 1$. Hence the intensity of the radiation will increase if $\alpha L > \gamma$. When this condition is achieved the oscillations continue to grow until the upper state is depleted to such an extent that the value of α no longer exceeds this critical value. It is important here to recall, from Fig. 2, that α is proportional to the product of the radiation density and the population excess.

A slightly different statement of the threshold condition is given in reference (5) and is as follows. If the transmission coefficient of the partial reflector is denoted by t, then on each two-way passage of the light through the cavity a fraction t of the light leaves the laser cavity. The intensity according to equation (11) changes by a fraction $\exp 2(\alpha L - \gamma)$. Therefore the light will be emitted from the laser at the rate

$$P = n h \nu \phi L [1 + \exp 2(\alpha L - \gamma) + \cdots] = \frac{n h \nu \phi}{[1 - \exp 2(\alpha L - \gamma)]} \qquad (12)$$

Hence the output would become infinite if $\alpha L \geq \gamma$. A steady output is maintained if the peak value α_m remains just below

$$\alpha_m = \gamma / L \qquad (13)$$

This equation represents the threshold condition.

As indicated in the discussion of Fig. 2, $\alpha = -k_\nu$ for the condition of population inversion. The variation of $\alpha(\nu)$ as a function of frequency is shown in Fig. 3. Hence the value of $\alpha(\nu)$ is at or below the peak value α_m over a very narrow range of frequencies. Therefore the output of the laser will be sharply peaked, and the bandwidth will be much more narrow than the atomic linewidth.

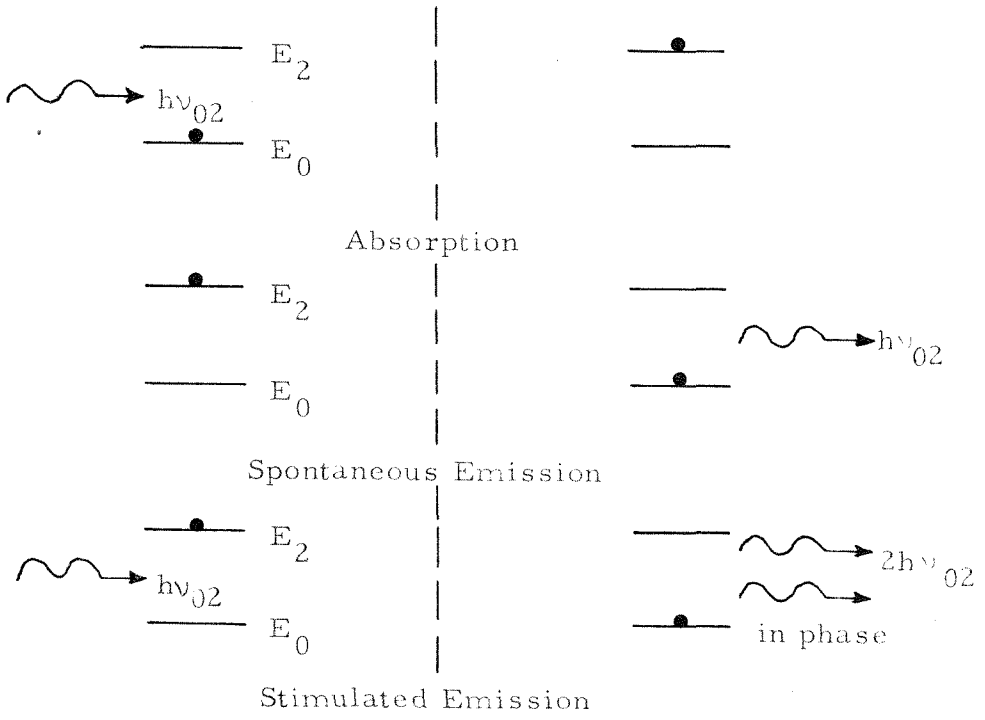

Fig. 1. Three basic transition processes between two energy levels.

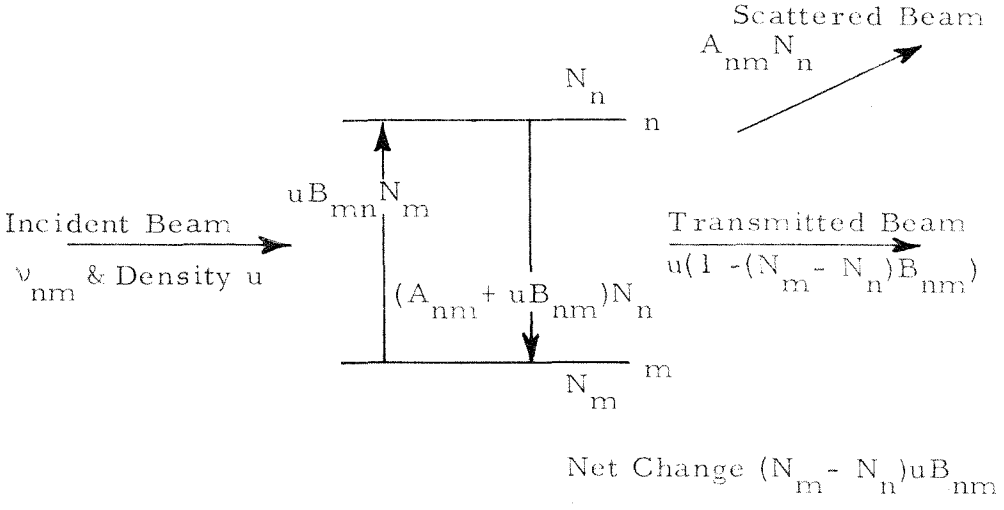

Fig. 2. Transfer of radiation in a two level system.

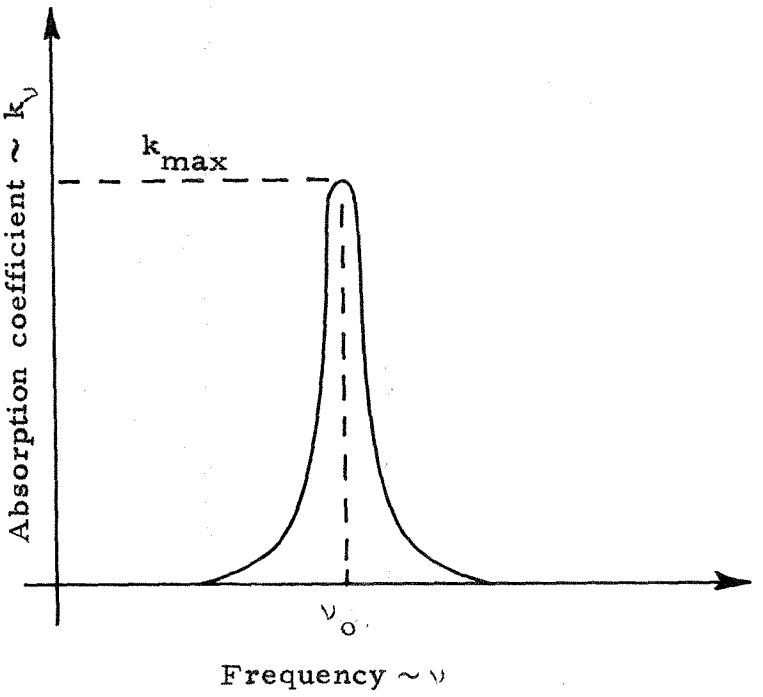

Fig. 3. Variation of absorption coefficient with frequency in an absorption line.

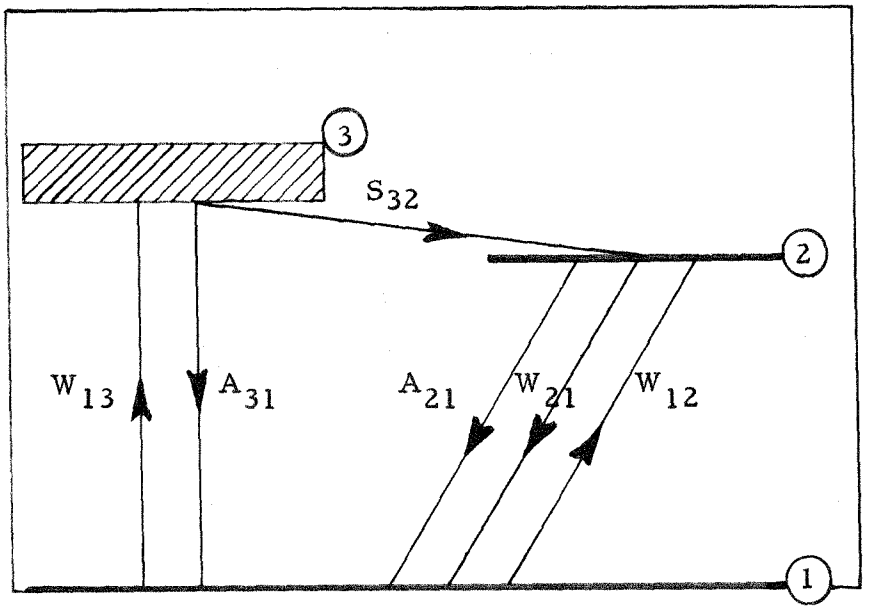

Fig. 4. Optical energy-level diagram for a three-level fluorescent solid. (Taken from Physical Reviews, reference 13).

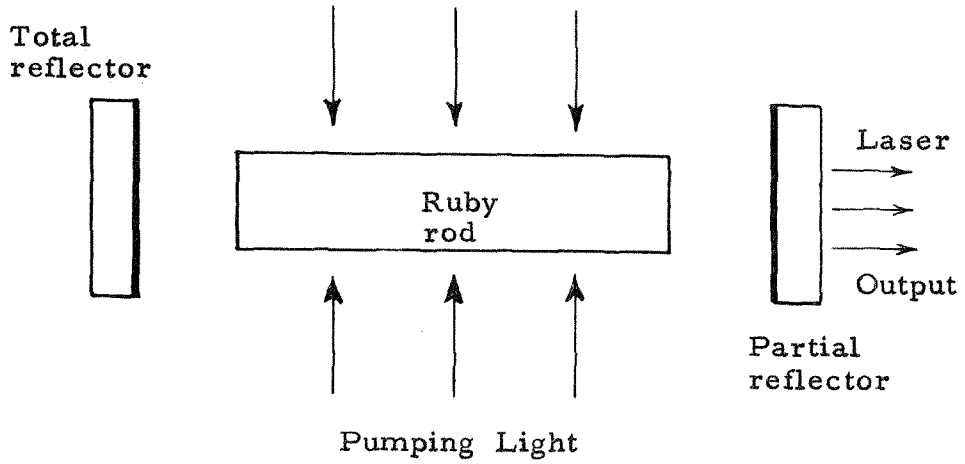

Fig. 5. Schematic diagram of laser.

SECTION B: DESCRIPTION OF LASER USED IN EXPERIMENT

I. Active Material

In the previous section the operation of a laser has been considered from the general point of view of a three level fluorescent solid. In this section the operation will be described for the particular solid used. In particular, the active material used throughout the course of this investigation was ruby (Al_2O_3) doped with 0.05 o/o Cr^{+3} ions. The essential portion of the energy diagram for this material is given in Fig. 6. The designation of the three levels taking part in the lasing action corresponds to that used in the previous section. The essential features are the two broad pumping bands, denoted by 3, and the split ^2E long lived state. Transitions from this level to the ground state are denoted by R_1 and R_2, but ordinarily lasing action takes place only at the R_1 line. The lifetime of this transition is given by Maiman [14] as 3.0 msec at 300° K and 4.3 msec at 77° K. He also obtained the absorption spectrum of ruby and this is shown in Fig. 7. The essential part is the location of the two broad peaks in the visible range corresponding to the broad pumping bands of Fig. 6. The spectral distribution of the Xenon pumping light is quite uniform over the visible spectrum, hence a poor efficiency may be expected from a coupling of this spectral distribution to the absorption characteristics of ruby. A pumping light which was blue or green would have been more efficient; however, the overall efficiency of the laser is quite low and electrical power is quite inexpensive, hence this was not a problem. In fact additional efficiency was sacrificed for the convenience of operating at room temperature. This absorption coefficient for the R_1 line at room temperature is $k_o = 0.4\ cm^{-1}$. [5] The location of this absorption line is shown in Fig. 7 as well as in Fig. 6, the energy diagram. The use of reciprocal cm for an energy unit, as shown in Fig. 6, is widespread in the laser literature. The origin of this unit is the relationship given in equation (1), which may be written

$$\frac{1}{\lambda} = \frac{E_2 - E_1}{hc} \qquad (14)$$

The numerical value of hc is 1.986×10^{-16} ergs cm.

The crystalline structure of the ruby has rhombohedral symmetry. The optic axis coincides with the axis of rotation of the threefold element of symmetry. In the ruby used the optic axis was at 90^{o} to the rod axis.

II. Operation in the Free Running Mode

The optical coupling of the ruby to the pumping flashtube was accomplished by using a cylindrical cavity of elliptical cross section. The ruby rod was located at one focus of the ellipse and an EGG FX-42 Xenon flashtube at the other. This arrangement is shown in Fig. 8 which is a schematic drawing of the laser cavity. In Fig. 9 the actual laser is shown; it will be noted that the walls of this cavity are highly polished in order that a high degree of optical coupling might be achieved. All ruby rods used were 1/4 inch diameter and 3 inches long.

The Fabry-Perot interferometric cavity was formed between a reflector on the back end of the ruby rod and an external dielectric mirror. The transmission properties of this mirror were determined and are given in Fig. 10. The reflectivity at $6943A^{o}$ is 90 o/o. A majority of the tests were conducted using a TIR (totally internal reflecting) ruby rod. This consisted of a wedge end cut at such an angle that any light propagating along the rod axis would be totally reflected in a direction parallel to the incoming ray.

The pumping circuit for the FX-42 flashlamp is shown in Fig. 11. In general the pumping energy input was less than 1280 joules. The minimum threshold energy was 160 joules, however, this value was increased slightly for different configurations of the laser cavity. An accurate measure of the input energy was not obtained.

The typical output of the laser is shown in Fig. 12 along with a record of the pumping light. The characteristic delay for population inversion to be achieved will be noted. The output will be

noted to be quite irregular in the free running mode which has been explained as partially due to the fact that a laser is a multimode cavity in which oscillations arise and decay in different modes at different rates.[5] In section D it will be seen that although the amplitude varies in such a random manner it is quite useful for taking single pictures and results in most cases in a significant improvement over standard methods, a result of the inherent properties of the laser light.

III. Operation in the Pulsed Mode

The major problem that had to be overcome to make the laser useful for high speed photography was that of converting the random output, as shown in Fig. 12, to one that could be controlled. The general requirement was that the laser should give an output only when commanded to do so. The general method by which this was approached was by a Q spoiling* technique. Two parallel programs were begun: (a) using a Kerr cell as a Q spoiler, (b) using a rotating mirror within the laser cavity as a Q spoiler. Although both programs were successful, the former offered many advantages and resulted in the discontinuation of the latter.

The laser with the Kerr cell inserted in the cavity is shown in Fig. 13. The purpose of the Kerr cell is to rotate the direction of the polarized light which is propagating in the laser cavity and effectively increase the loss coefficient. That is, the mode which would normally be built up is actually suppressed due to the change in the direction of polarization of the light. The axis of the Kerr cell was placed at 45° to the optic axis of the ruby and operated in the on-off-on mode. Therefore during the output pulse the Kerr cell was completely inoperative and did not affect the properties of the laser light.

Q spoiling by means of a rotating mirror was accomplished as

* The term Q spoiling is a carry-over from other areas of electronics and implies a means of increasing the losses in the cavity.

this mirror was required to be in the proper position for the laser cavity to be complete.

A phenomenological description of how Q spoiling is achieved within the active material may most easily be approached by considering the loss coefficient as a function of time. The threshold condition was given in section A as:

$$\alpha_m = \gamma/L \qquad (13)$$

The amplification coefficient $\alpha(\nu)$ is related to the population excess by

$$\alpha_{12} = (N_2 - N_1)\sigma_{12} \qquad (15)$$

where σ_{12} is the absorption cross section for the pertinent transition. In this expression it is assumed that population inversion has already been achieved and therefore $N_2 > N_1$.

If the input power is assumed constant, after some given time a certain degree of pupulation inversion will have taken place. Hen if lasing action has not begun, the population excess will be fixed, and therefore the amplification coefficient will be fixed. Lasing action will not take place until the loss coefficient γ is at such a value that the threshold condition may be met. If the value of γ may somehow be increased so that the threshold condition can not be met a corresponding increase in the population excess may be achieved. Now if γ is suddenly decreased to a value much lower than the value required by the amplification coefficient for a thres hold condition lasing action will begin and the stimulated transitio will be accelerated due to the excess population inversion and the high radiation density. The population excess will rapidly be reduced to a value less than required for the lower value of the thr hold condition and lasing action will be terminated.

The Kerr cell was filled with nitrobenzene and operated at a voltage of 10 KV. The voltage pulse to the Kerr cell is shown in Fig. 14. The duration of this pulse is seen to be 0.1 μsec and the rise time is approximately 20 nsec. The duration of this pulse could be altered at will.

The output of the laser operating in the pulsed mode is shown in Fig. 15. This pulse is one of a series when the laser was operating at a repetition rate of 500 kc. The rise time is approximately 10 nsec. Due to this rapid rise time and the high intensity of the pulse accurate detection was somewhat of a problem. After trying several photosensitive devices an ITT FW-114A photodiode tube was used and good results were obtained. This photodiode operates at an anode voltage of 2.5 KV and has a linear output up to 5 amps. The rise time of this cell is quoted to be 2 nsec. To obtain a comparably short rise time with the viewing system, it was necessary to bypass the amplifier of the oscilloscope, which had a rise time of 7 nsec, and insert the input directly on the plates of the cathode-ray tube which had a rise time of 1.5 nsec. This arrangement is shown in Fig. 16; it may be noted that special precautions were taken to insure a minimum rise time in the accompanying circuit. As a result it is felt that the trace shown in Fig. 15 accurately represents the output of the laser in the pulsed mode at this power level.

McClung and Hellwarth[15] were the first to achieve a "giant" pulse from a ruby laser. In their experiment a Kerr cell was used as a Q spoiling device and a single pulse was obtained. Their interest was in studying the details of the laser pulse to obtain an insight into the phenomena involved.

For use in high speed photography it was necessary to generate a series of light pulses. This required that the Kerr cell be pulsed to key the laser. It should be remarked here that work on this phase of the experiment was in the final phase when the information concerning the generation of a single pulse by this method was published (March, 1962) in reference (15).

IV. Results for Pulsed Mode

The results of operation of the laser in the pulsed mode were as follows.

In the first place, the primary objective of this investigation was accomplished. That is, a method for control of the laser output was devised. This point of view will be considered in more detail in section D , where applications are discussed.

Secondly, in the course of achieving the first objective, several interesting aspects were noted. The pulse train generated by the Kerr cell method of Q spoiling was found to have the following properties. The pulse amplitude stabilized above a certain critical repetition rate which was found to be a function of the cavity length. Several examples of series of light pulses generated by this method are shown in Fig. 17. The details concerning repetition rates and cavity lengths are summarized in Table I. The time span covered by these pictures is not the total lasing period. In general, the time delay between the initiation of the pumping light and the start of the sweep in each of the records of Fig. 17 is constant.

The amplitude variation that will be noted in Fig. 17 was of particular interest. A parametric study of the effect of repetition rate and external mirror separation on the pulse amplitude was made. The results of these tests are presented in Fig. 18. Two effects are noted: (a) a decrease in amplitude with increasing repetition rate, and (b) a decrease in amplitude with increase of cavity length.

The first effect may be explained in the following manner. Assume, for the time of interest, that the pumping power is constant (this is approximately true, as may be seen in Fig. 12-a). Therefore, the number of ions which are pumped from the ground state into an excited state per unit time is constant. Transitions to lower levels will occur as described in section A. Hence, the population of ions in the long lived state is a direct function of the pumping time. The number of ions available for lasing action is therefore directly proportional to the repetition rate. That is, this may be viewed as a stabilized rate process. If this type of mechanism is responsible

for the observed behavior, then the curves shown in Fig. 17 should have the general form:

$$(P - P_o) = \frac{K}{(R - R_o)} \qquad (16)$$

where P is the peak power and R is the repetition rate. P_o, R_o, and K are constants determined for each curve. The general agreement between the experimental data and this empirical equation is shown in Fig. 18.

The amplitude variation with cavity length may be explained as a variation in the number of modes excited within the laser cavity. The output of the laser consists of photons which on the average have completed 10 round trips of the laser cavity (the number of passages is a function of the reflectivity of the partial reflector). When the cavity is lengthened, fewer photons are emitted in the direction required for amplification.

The next characteristic of this series of light pulses to be investigated was the duration and shape of a single pulse. A typical pulse is shown in Fig. 19. This represents an input energy of 1280 joules, with the Kerr cell operating at 1.2 Mc and an active period of 0.1 μsec for the Kerr cell. The active period, or pulse duration, for the Kerr cell was varied from 0.1 to 0.4 μsec, which represents approximately half of the quiescent period. Figure 19 shows that this had no effect on the duration or shape of an individual pulse. The same procedure was carried out to determine the effect on the amplitude stability of the pulse train. Figure 20 shows that the effect is small, although noticeable, for long Kerr cell pulse duration.

As a result of these last two tests, it is concluded that the length of the light pulse is independent of these parameters for the range investigated. The duration of this pulse appears to be a function only of the active material, the pumping power level, and the efficiency of Q spoiling in the laser cavity. The output of this laser was less than one joule. Results from limited tests on this low energy laser as well

as discussions with investigators using higher energy units indicate that if the power level were increased by a factor of ten, the pulse duration could be expected to decrease to several nanoseconds.

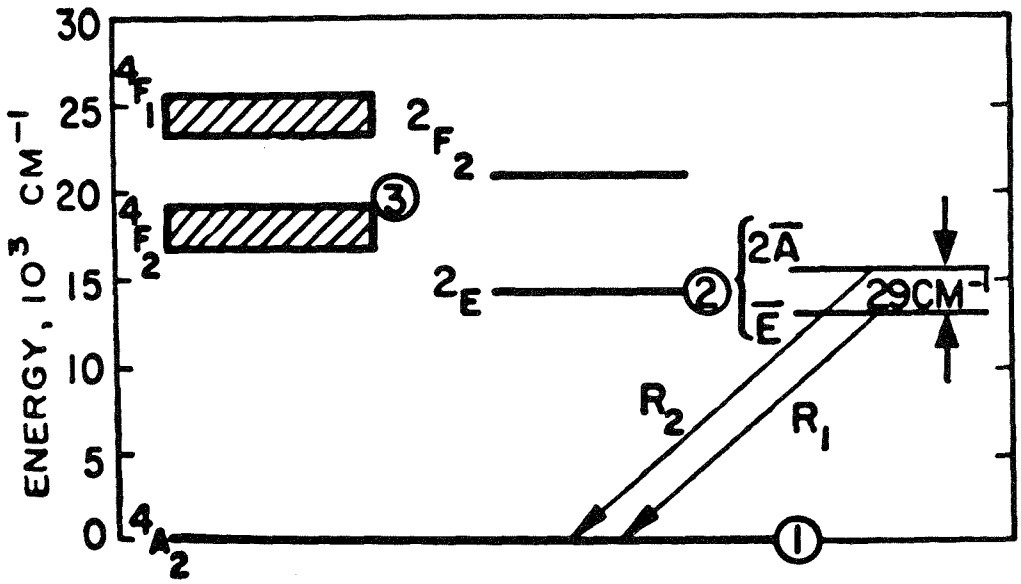

Fig. 6. Energy-level diagrams for ruby (taken from Physical Reviews, reference 5)

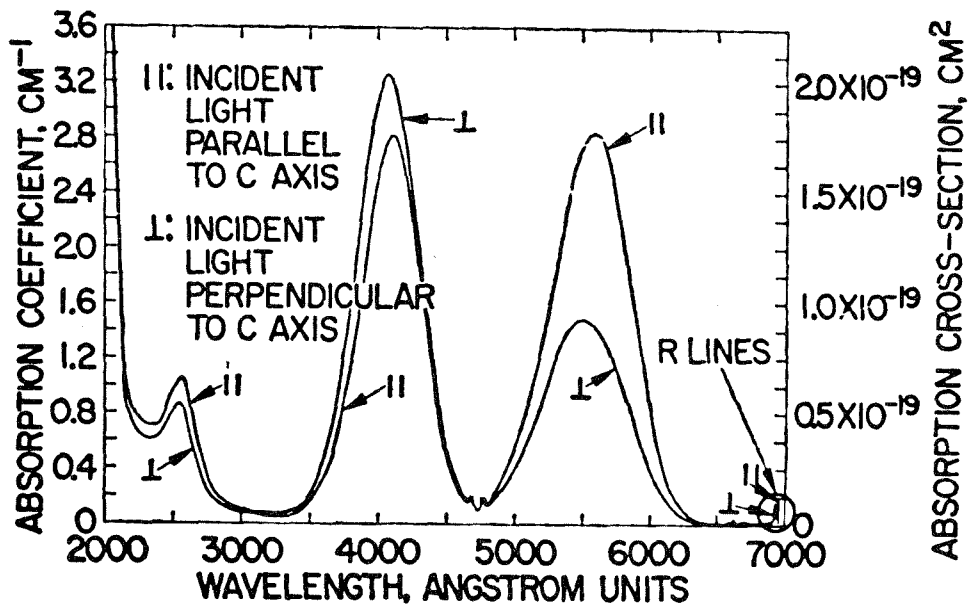

Fig. 7. Spectrophotometric absorption spectrum of ruby. (Taken from Physical Reviews, reference 5)

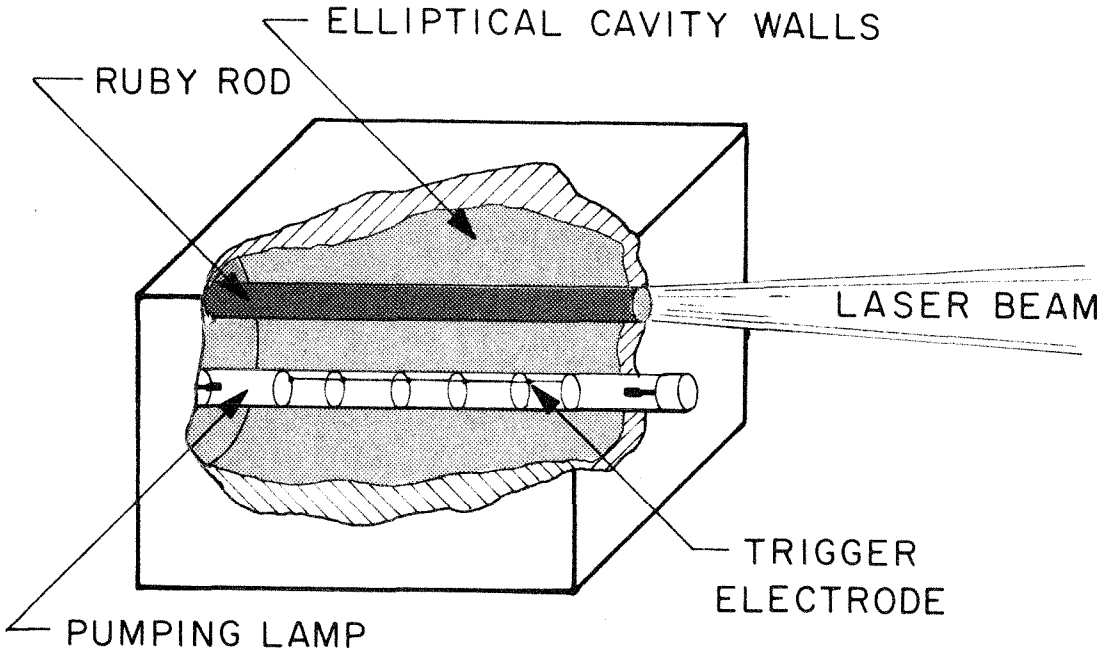

Fig. 8. Schematic of ruby laser with cylindrical cavity of elliptical cross section.

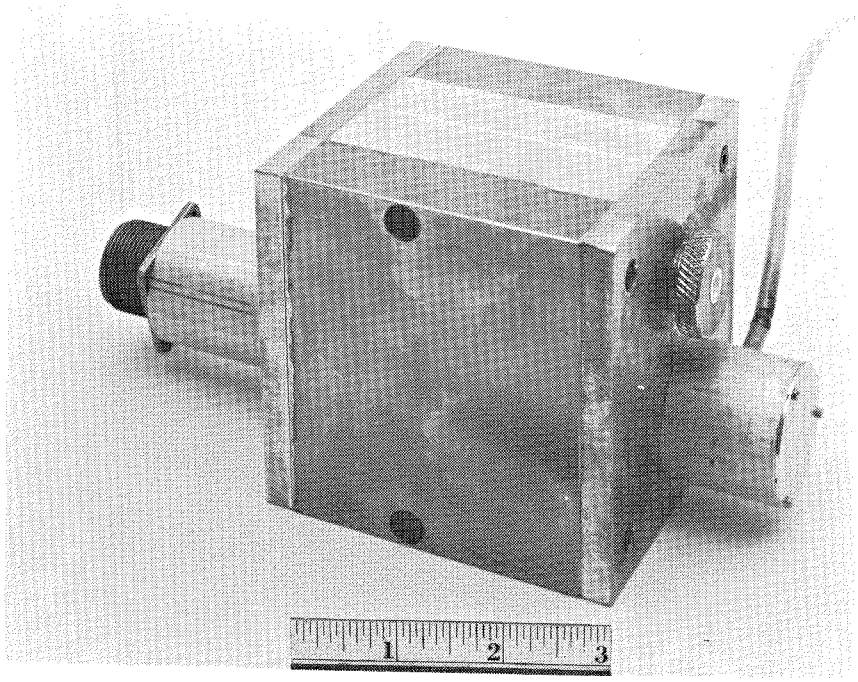

(a)

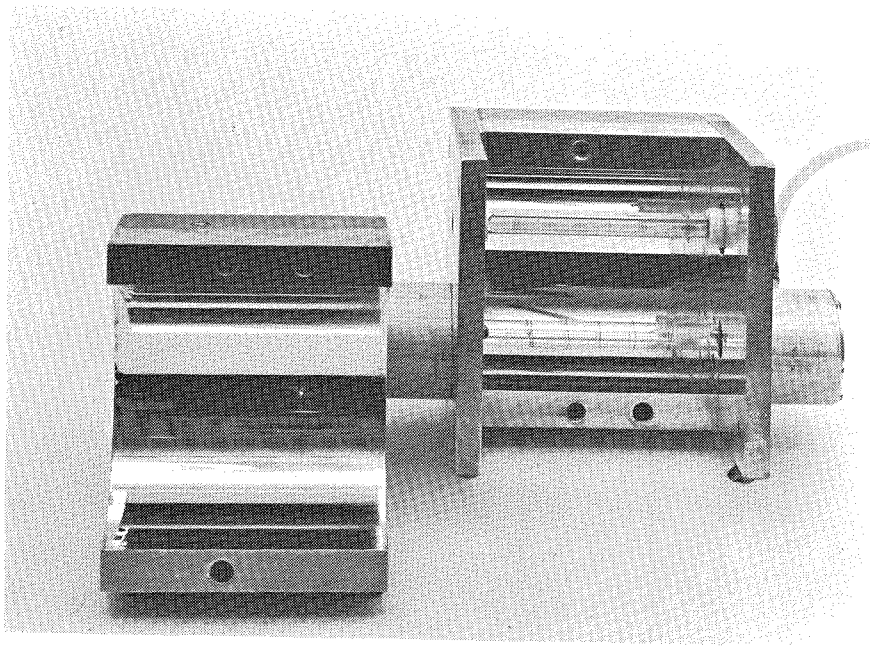

(b)

Fig. 9. Details of laser cavity; (a) external, (b) internal view with ruby rod and pumping flashtube exposed.

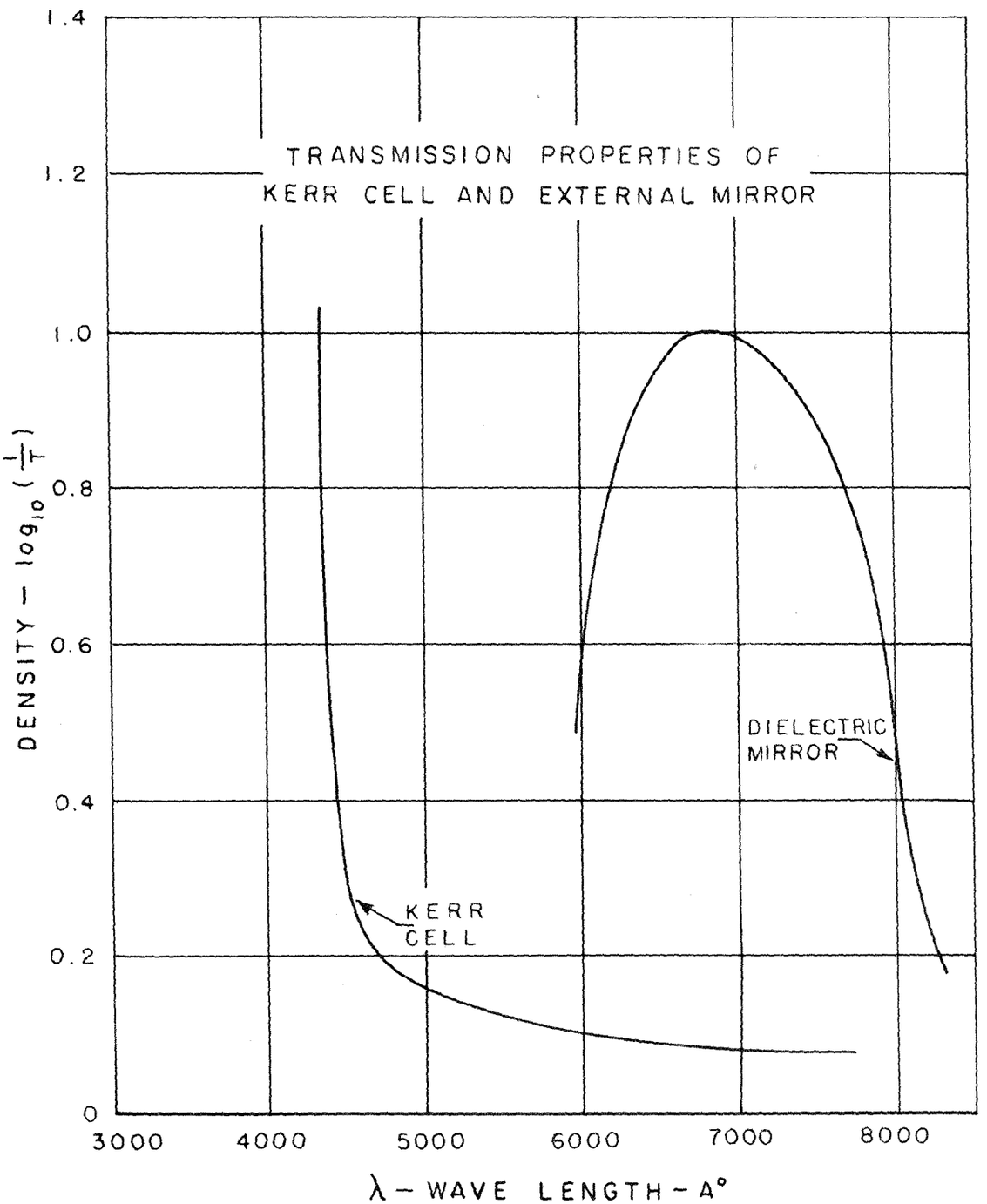
TRANSMISSION PROPERTIES OF
KERR CELL AND EXTERNAL MIRROR
DENSITY − $\log_{10}(\frac{1}{T})$
1.4
1.2
1.0
0.8
0.6
0.4
0.2
0
3000
4000
5000
6000
7000
8000
λ − WAVE LENGTH − A°
DIELECTRIC MIRROR
KERR CELL

Fig. 10

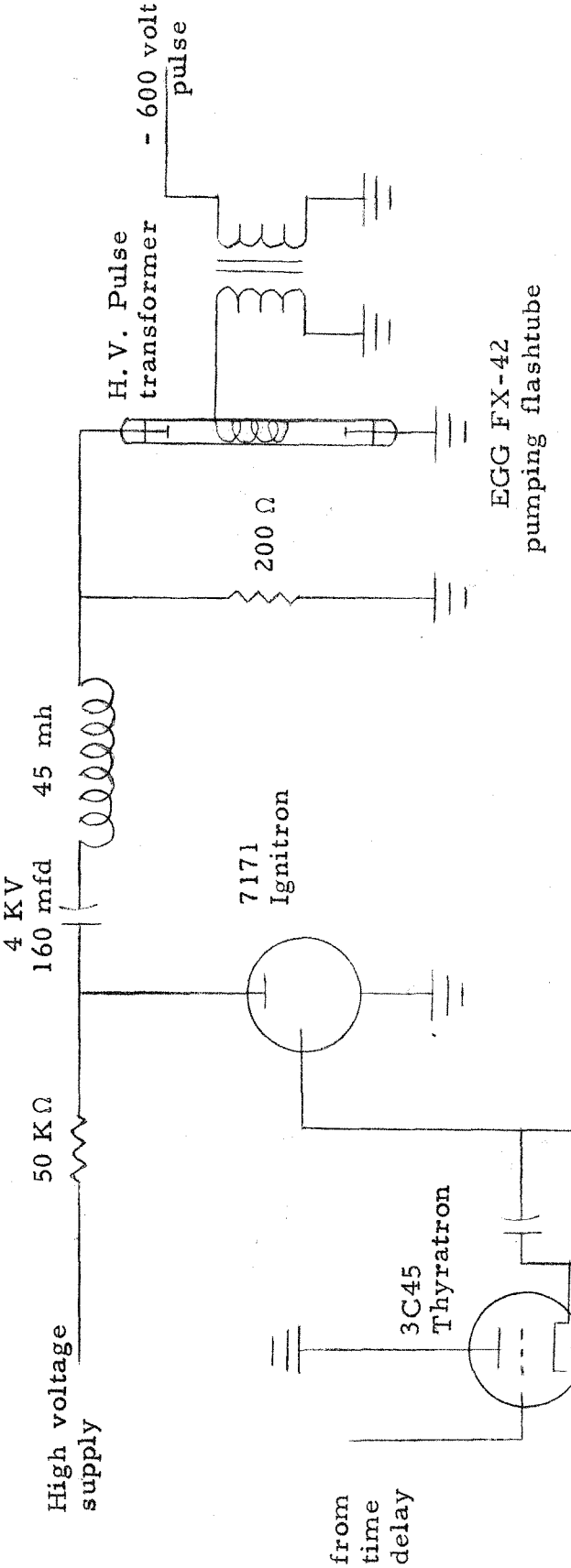

Fig. 11. Laser pumping flashtube circuit.

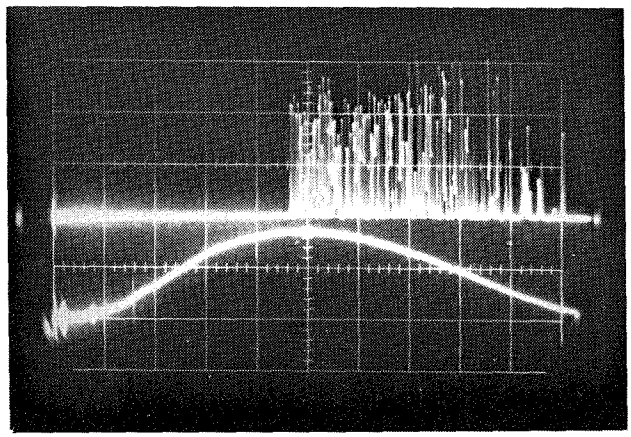

(a)

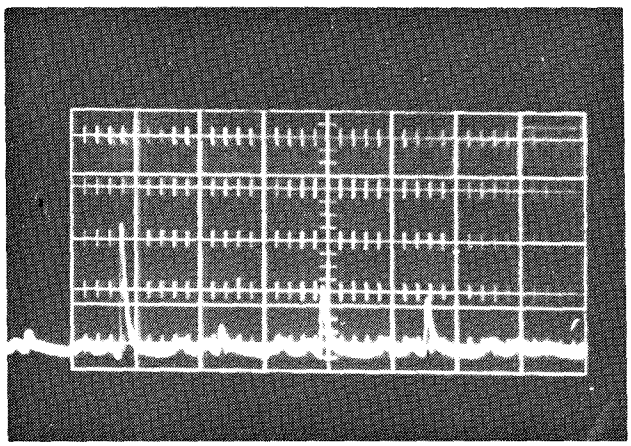

(b)

Fig. 12. Laser output in freerunning mode. (a) Sweep speed of 200μsec/cm, top trace is laser output, lower trace is pumping light. (b) Laser output with time scale expanded to 0.5μsec/cm.

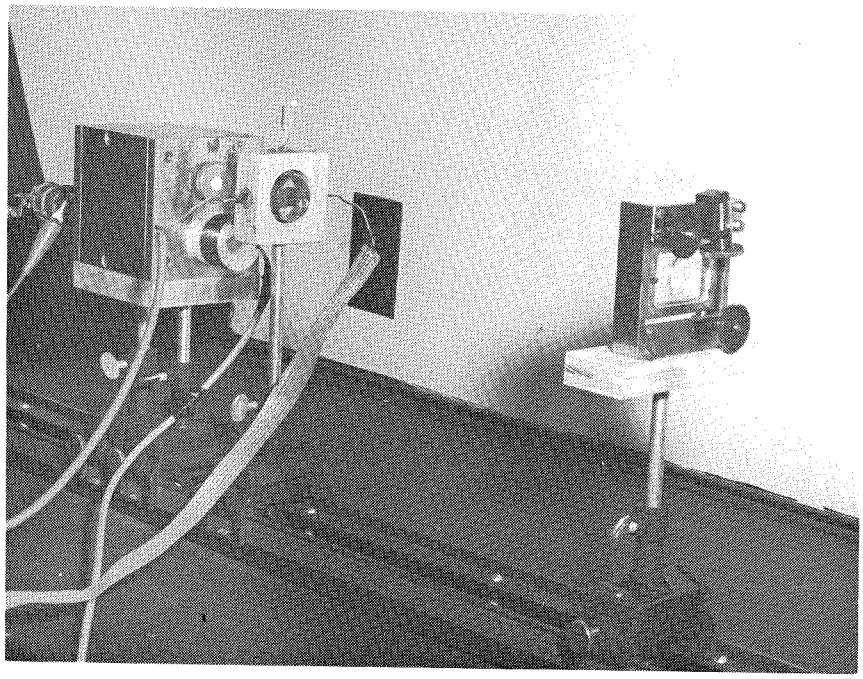

Fig. 13. Laser with Kerr cell inserted in cavity and moveable external mirror.

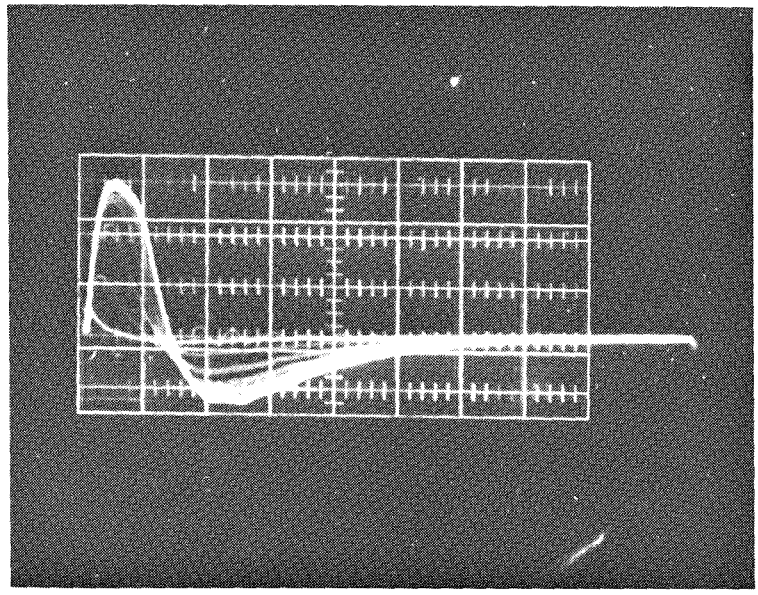

Fig. 14. Kerr cell voltage pulse. Sweep speed 0.1μsec/cm.

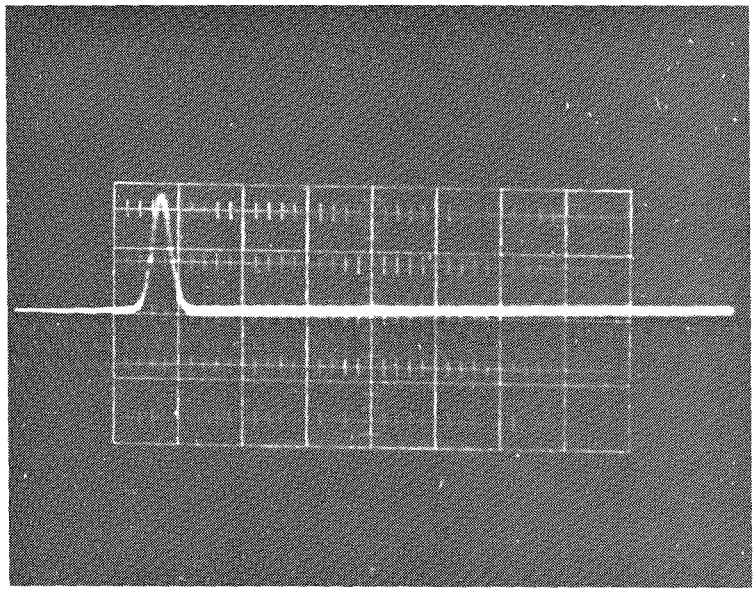

Fig. 15. Laser light pulse at repetition rate of 500 kc, sweep speed of 0.1μsec/cm.

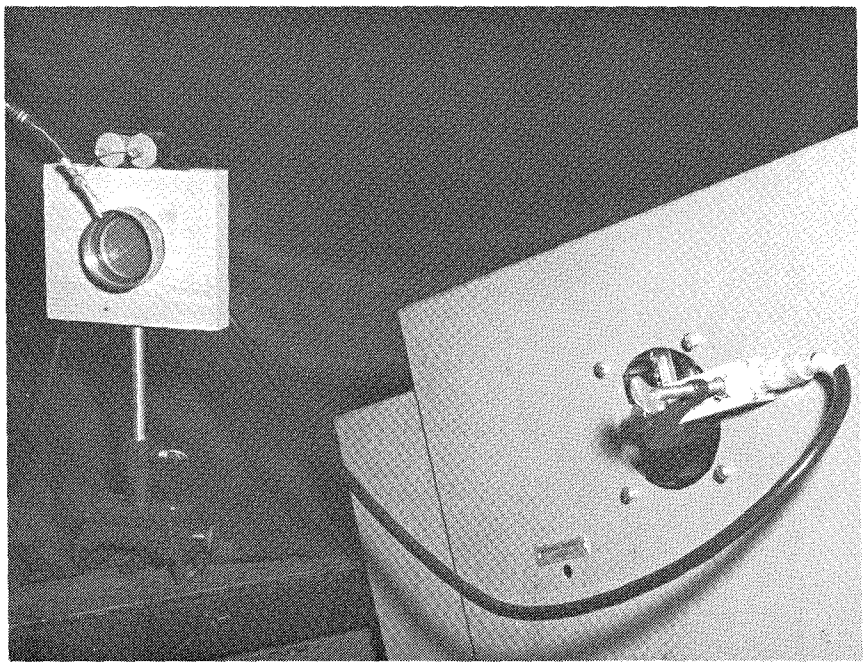

Fig. 16. Photodiode (ITT FW 114a) shown with input connected directly on oscilloscope plates.

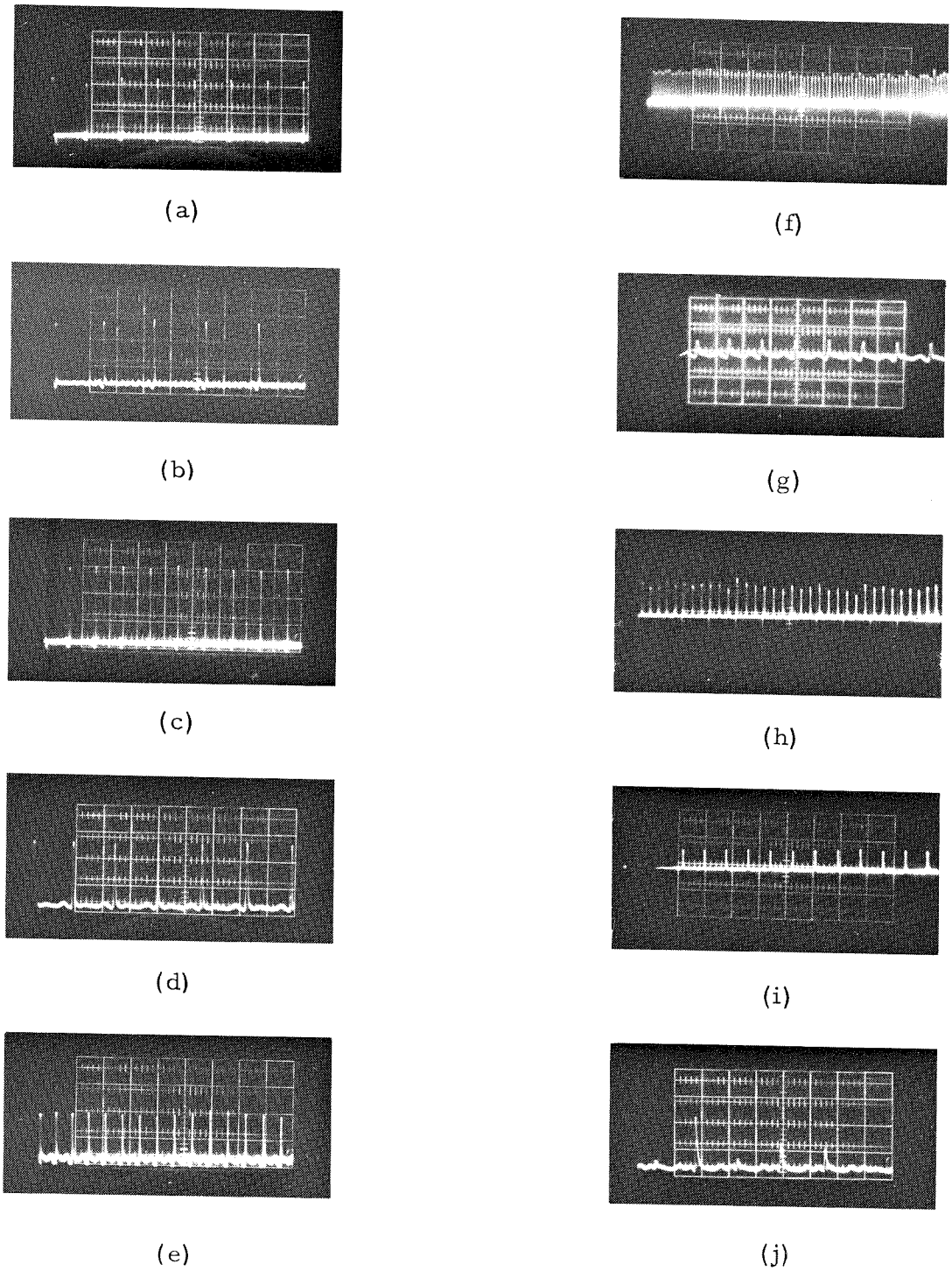

Fig. 17. Stabilized laser pulse amplitude for various repetition rates and cavity lengths. For details see Table I.

Fig. 17-	Oscilloscope Sweep Speed	Laser Pulse Repetition Rate	External Mirror Separation
a	2μsec/cm	353 kc	24 cm
b	1μsec/cm	480 kc	24 cm
c	2μsec/cm	500 kc	24 cm
d	0.5μsec/cm	1.2 Mc	24 cm
e	1μsec/cm	1.5 Mc	24 cm
f	5μsec/cm	1.4 Mc	44 cm
g	0.5μsec/cm	1.66 Mc	44 cm
h	5μsec/cm	600 kc	54 cm
i	1μsec/cm	1.14 Mc	34 cm
j*	0.5μsec/cm	free running	24 cm

* Gain same as (d)

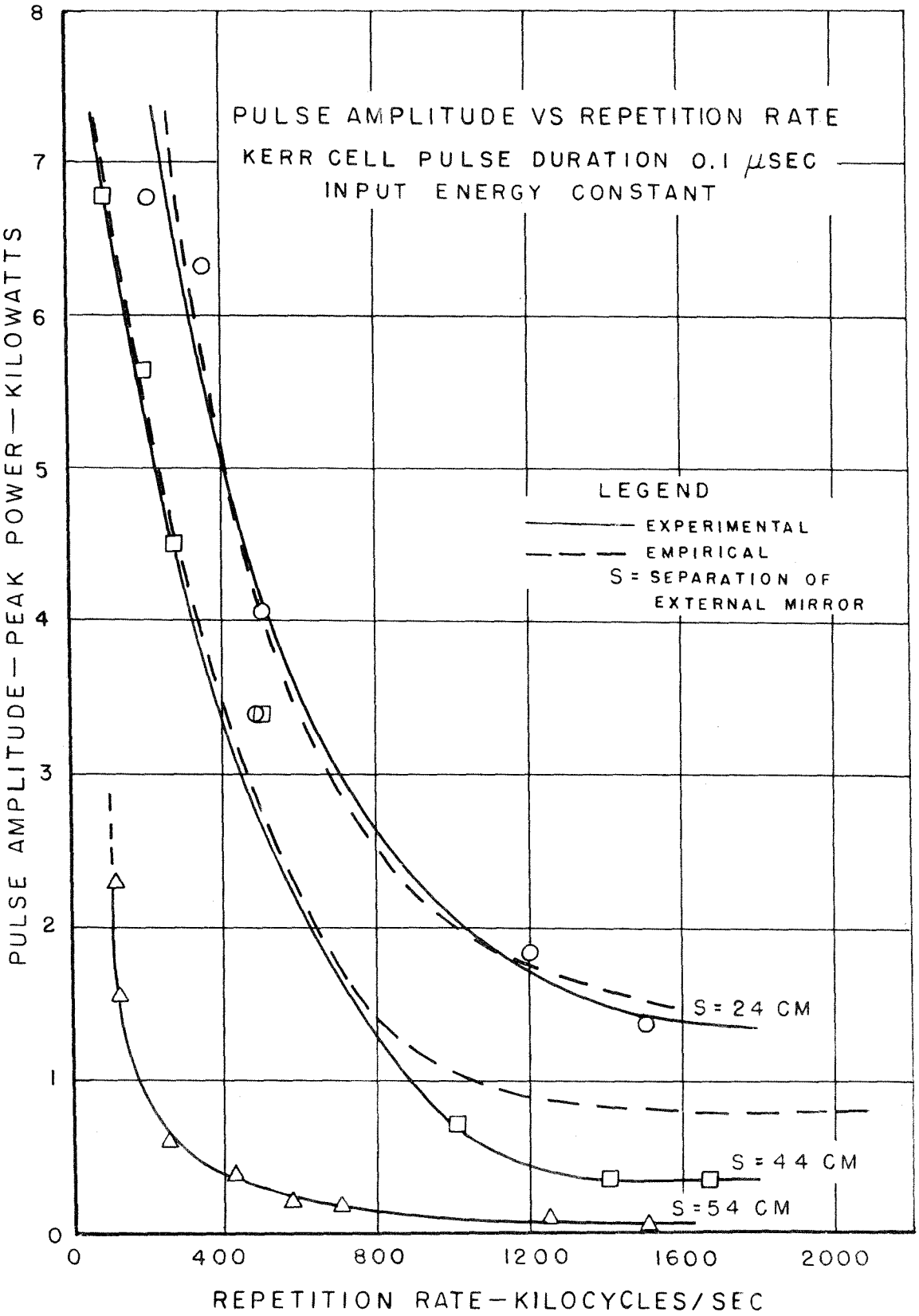
PULSE AMPLITUDE VS REPETITION RATE
KERR CELL PULSE DURATION 0.1 μSEC
INPUT ENERGY CONSTANT
LEGEND
EXPERIMENTAL
EMPIRICAL
S = SEPARATION OF EXTERNAL MIRROR
S = 24 CM
S = 44 CM
S = 54 CM
PULSE AMPLITUDE — PEAK POWER — KILOWATTS
REPETITION RATE — KILOCYCLES/SEC
0
1
2
3
4
5
6
7
8
0
400
800
1200
1600
2000

Fig. 18

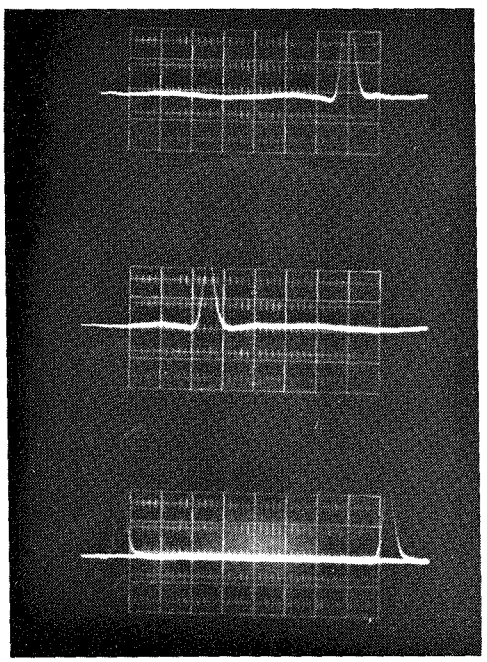

Fig. 19. Laser pulse duration and shape as function of Kerr cell pulse duration. Sweep speed 0.1μsec/cm. (a) Kerr cell pulse duration 0.2μsec, (b) 0.3μsec, (c) 0.4μsec.

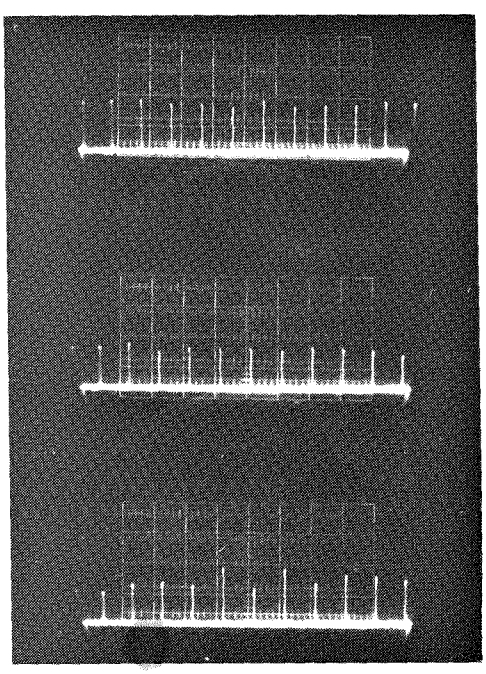

Fig. 20. Laser pulse amplitude stability as function of Kerr cell pulse duration. Sweep speed 2μsec/cm, repetition rate of 500 kc. Kerr cell pulse duration (a) 0.1μsec, (b) 0.2μsec, (c) 0.3μsec. (Note: Gain is not the same in these three cases.)

SECTION C: CAMERA

This discussion will be limited to the specific camera that was built to be used in conjunction with the laser. Several other standard ones were used in the course of this investigation; however, they were used only to demonstrate specific aspects of the laser.

The laser when operating in the pulsed mode acts both as a light source and a shutter. Therefore in principle the camera may be quite simple. The major requirement, other than an acceptable optical system, is a means of obtaining a physical separation of each frame on the film. In all cases some form of a rotating mirror was used for this purpose. In the design of the camera to be used with the laser the following aspects were considered.

(a) The high intensity of the laser light made it possible to have a large area of film exposed.

(b) The collimated nature of the light adapted itself easily to a variety of optical systems.

(c) The extremely short duration of the light pulse made high image speeds over the film plane possible.

(d) The inherent properties of the light from a laser made several areas of research via photographic means desirable. That is, the monochromaticity and linear polarization of the light makes it very desirable for high speed photoelasticity. The collimated nature is useful in Schlieren photography, etc.

The camera that was built to be used with the laser is shown in Fig. 21. It will be noted that this camera differs from standard high speed cameras in two major points. First, the optical lever arm is much longer than normal. Thus the image may be swept across the film at speeds greater than 10^6 inches per second, enabling one to obtain a large frame separation. Secondly, the film used is 9 1/2 inch aerographic film.

Figure 22 is a schematic of the optical arrangement used.

The long optical lever arm places somewhat severe requirements on the optical quality of the rotating mirror. It was found that the flatness tolerance required was within one fringe (in green light). Distortion due to initial irregularities were more severe than those due to rotation.

A block diagram of the electronic arrangement of the entire camera system is shown in Fig. 23. The major point to be noted is that due to the characteristic time delay necessary for population inversion to be achieved in the laser, the entire sequence of events must be synchronized. This point, in fact, affected the design of the camera in that a quadrant of a circle was used rather than a full circle. The initiation of the timing sequence is obtained from a signal from the rotating mirror. The remaining sequence is shown in Fig. 23.

In passing we might note that an additional reason for designing a camera with such a high image sweep speed was an attempt to determine the duration of the light pulse. An upper bound was obtained in this manner and later verified by the photodiode as described in section B.

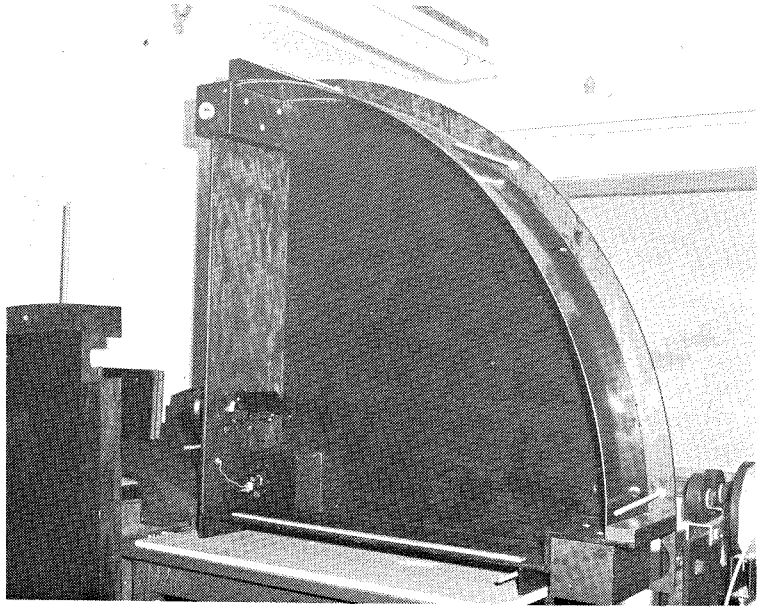

(a)

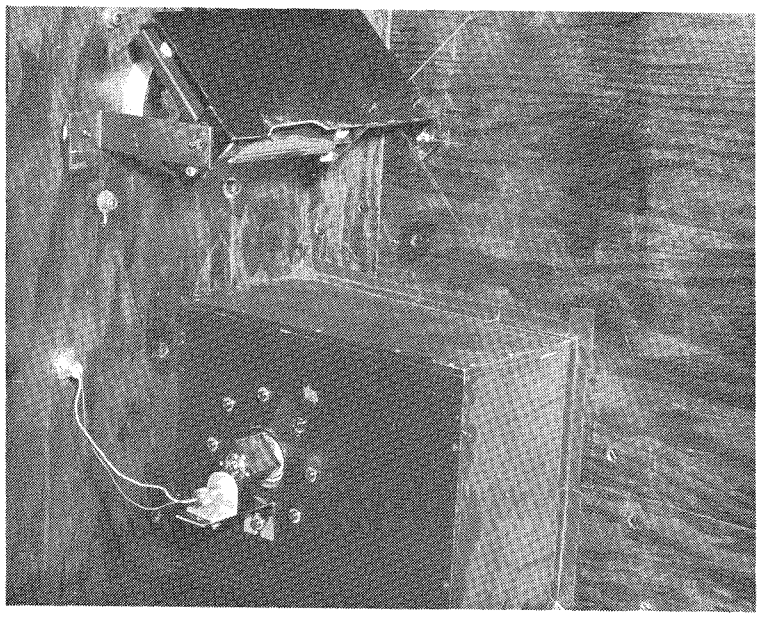

(b)

Fig. 21. High speed laser camera. (a) Overall view of camera with side removed. (b) Detail view of rotating mirror section of optical arrangement.

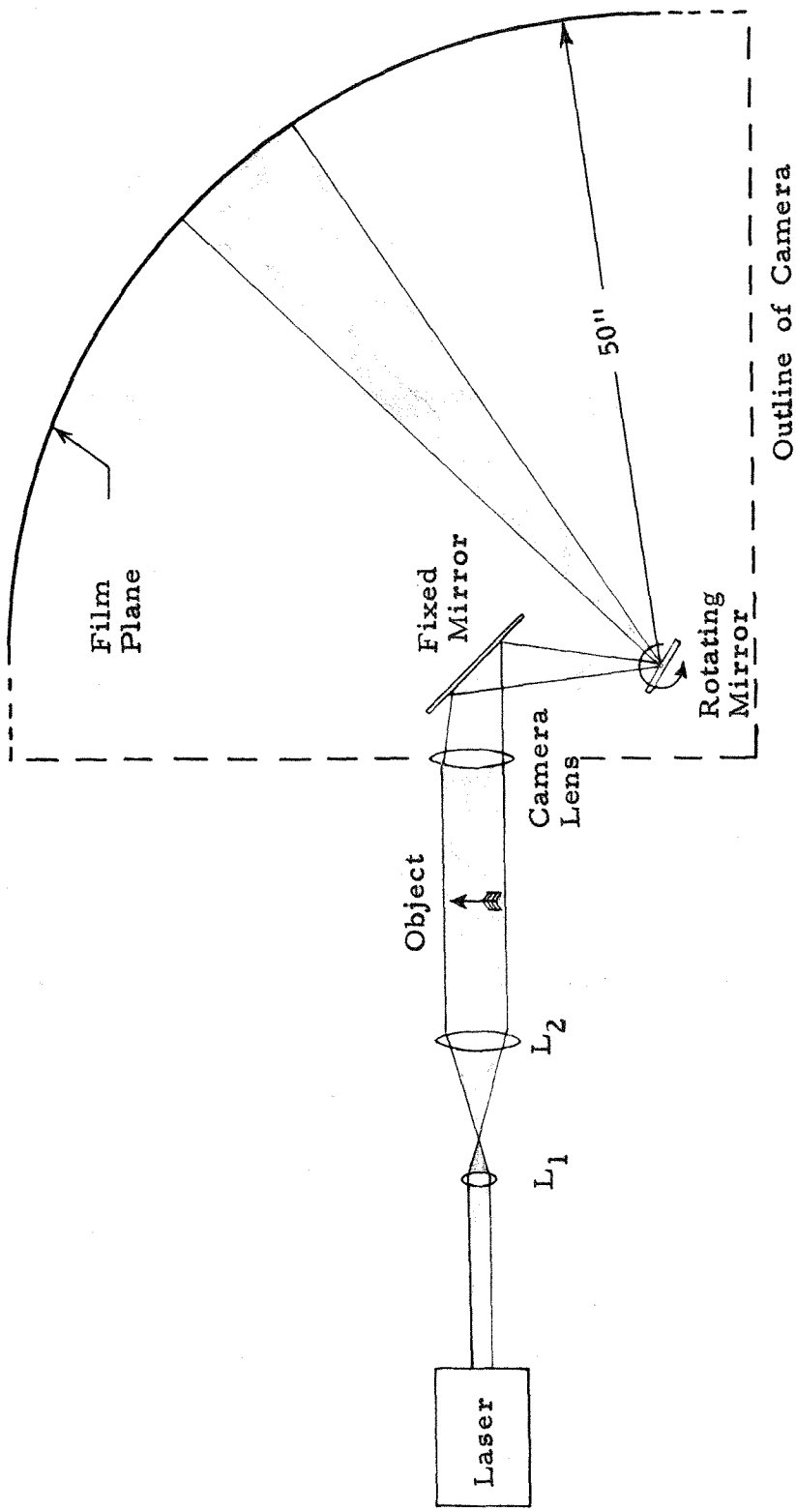

Fig. 22. Schematic of optical arrangement of camera.

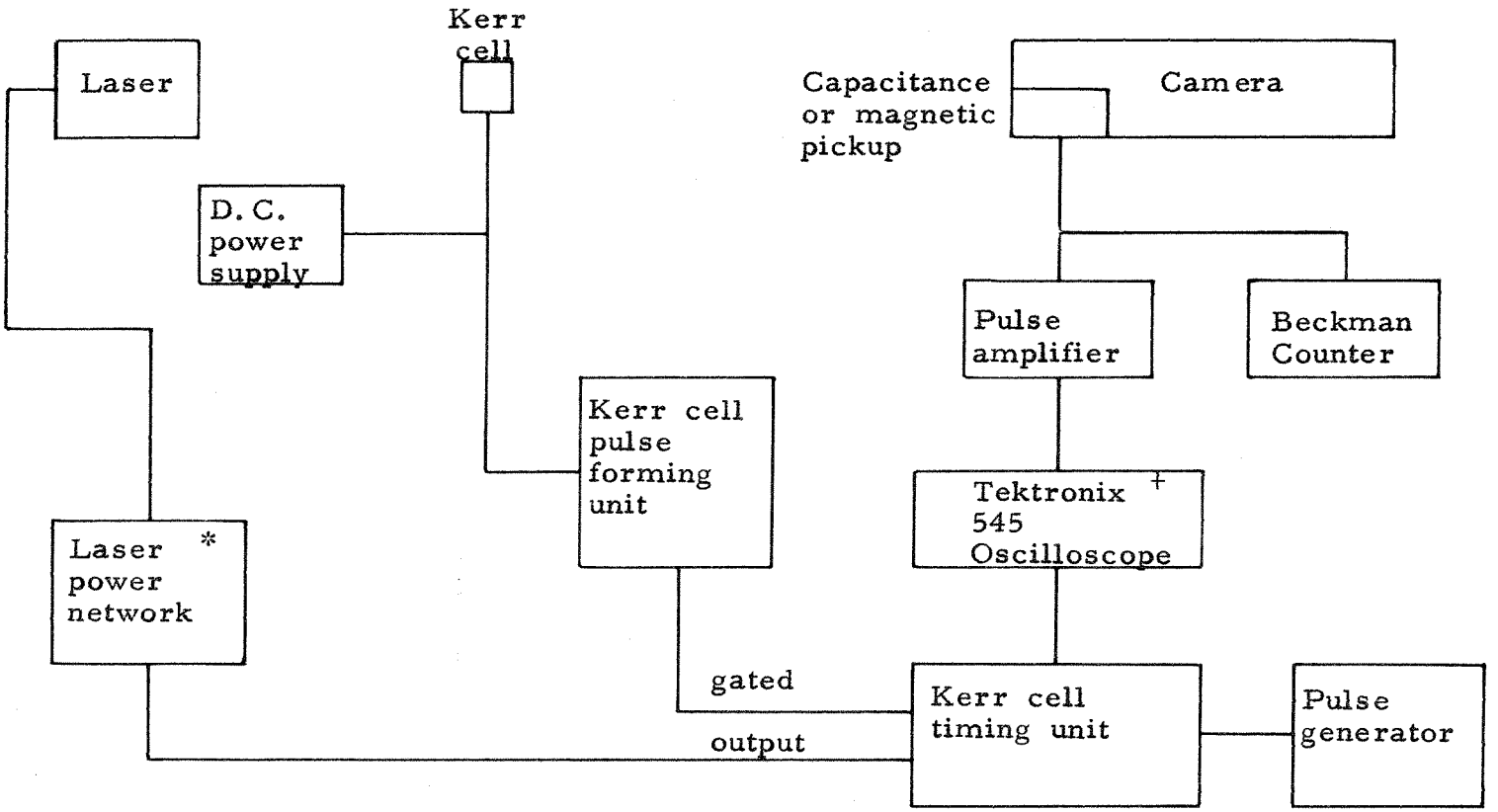

* For details see Fig. 11

\+ Used in single sweep mode to generate reliable timing signal

Fig. 23. Block diagram of high speed laser camera.

SECTION D: APPLICATIONS

I. Introductory Remarks

A general discussion of the possible applications of a laser, even when limited to the area of photography, would be exceedingly lengthy. Therefore this section will be limited to the particular applications which have been investigated. The primary aim of these investigations was to determine the desirable characteristics and limitations of the laser as a research tool. Therefore no effort has been made to solve particular problems but rather the emphasis has been placed on somewhat shallow investigations of broad areas.

In the last part of this section a few remarks will be included on some proposed applications.

II. Single Frame Operation

As a convenient means of obtaining information concerning the properties of the light generated by the laser several static pictures have been included. For these pictures the laser was operated in the free running mode; hence the exposure time was approximately 0.5 msec. The first problem to be investigated was that of choosing a film that could be used. The sensitivity of ordinary photographic films in the region of 7000 A° is quite poor. Therefore it was necessary to evaluate several rather exotic types of film. The results of this evaluation are summarized in Table II.

Although the exposure time for these pictures is long compared to that necessary for high speed photography the results obtained were quite meaningful. In part this is due to the significant increase in intensity of the laser output when operated in the pulsed mode. It also implies that the law of reciprocity was valid for the majority of the films tested, in the range tested. A quantitative measure of the actual degree of validity would be difficult to obtain. However, in general it may be said that the characteristics recorded in these static pictures will be present for short exposure

TABLE II

Type of film	Size tested	Quoted speed	Comments
Kodak 103-F spectroscopic	8X10 in. glass plates	log sensitivity of 0.8 at 7000A° *	Good, best of group tested for definition, sensitivity acceptable.
Kodak infrared aerographic, SP-885	9 1/2 in. X75 ft. roll film	ASA 125	Sensitivity good, however definition suffered due to lack of backing on film.
Kodak high speed infrared safety film SP-764	35 mm X 1000 ft. roll film	ASA 200	Same as aerographic except with backing.
Kodak 103-U spectroscopic	70 mm X 75 ft. roll film	log sensitivity of 1.4 at 7000A°	Inconvenient for use due to low temperature storage requirements. Showed tendency to fog easily.
Polaroid infrared	3 1/4 X 4 1/4 in. sheet film	ASA 800	Good sensitivity, however only available on special order.
Polaroid type 47	3 1/4 X 4 1/4 in. sheet film	ASA 3000	Sensitivity less than 103-F by factor of 5. Definition not as good as standard films, however quite convenient to use.
Kodak type 1-F	5 X 7 in. glass plates	log sensitivity of 1.3 at 7000A°	Essentially equivalent to 103-F, except slightly more sensitivity.

* Sensitivity is defined in Kodak Publication No. P-9.

dynamic ones as well.

In Fig. 24 a single bubble is shown, photographed in silhouette. The bubble is held stationary by means of an acoustical field. A picture taken with a high pressure mercury Osram lamp of the identical arrangement is included for comparison. This corresponds to the best picture possible using previous techniques. The important points to be noted about this photograph are (a) the extremely sharp definition of the bubble boundary and (b) the diffraction patterns that are present both due to the bubble and to small sources within the water. As will be noted in the mercury light this water (distilled and degassed) appears clear. As a result of the appearance of these patterns, an experiment was conducted to determine the quality of a picture obtained by scattered light from small particles in a fluid. A concentrated solution of polystyrene spheres (0.285 microns in diameter) in water was photographed using the forward scattered light. This is shown at a magnification of 50 in Fig. 25. The excellent results obtained here imply that this type of photography will be quite useful in the area of flow visualization by means of flow tracers. The chief advantage of the laser over ordinary light sources in this area is that the intensity is sufficient to allow extremely small particles to be used as tracers.

In the field of cavitation it would be desirable to have the ability of generating a bubble within a fluid without inserting any device into the fluid that would disturb the flow. An attempt to achieve this effect by focusing the laser beam at a point within a vessel of water was made. The results are shown in Fig. 26. As will be noted a cloud of bubbles was generated instead of the desired single one.

A quite limited investigation of the application of a laser to photoelasticity was made. Figure 27 shows a photoelastic specimen subjected to a concentrated load on its boundary. Although the quality of this picture is acceptable by ordinary standards it is somewhat poor in comparison with the results presented thus far. This is due to two reasons: (a) the picture shown was taken on

polaroid film (an unforgivable sin in the photoelasticity camp), (b) the quarter wave plates of the polariscope used were for 5600 A^{o} light rather than 7000 A^{o} light. This resulted in elliptically polarized light rather than the desired circular polarization. The former point is considered to greatly overshadow the latter in this particular case. However, when quantitative results are required the latter point can no longer be ignored.

III. Multiple Framing Operations

The initial series of experiments conducted in the dynamic operation was again designed to investigate the properties of the laser. In the following applications the laser was operated in the pulsed mode, therefore the exposure time was 30 nsec in all cases. The definition possible using a laser in the static mode has already been discussed in conjunction with Fig. 24. The definition possible when operating in the multiple framing mode is illustrated in Fig. 28. A portion of a microscope scale is shown at a linear magnification of 25. The distance between the scale divisions is 100 microns, the framing rate is 2×10^{5} frames/sec, and the image speed across the film plane is 2×10^{5} inches/sec. It will be noted that no pull of the image is evident, attesting to the short exposure time.

Figure 29 shows the generation of a bubble in water by means of an electrical discharge. This picture was taken on 35 mm film using the film drum from the Ellis Kerr cell camera. The loss of half the image is due to a wedge shaped rotating mirror that was used. The shock wave resulting from the generation of the bubble may be observed. At a later time reflected shocks from the bottom of the vessel as well as the surface of the water were observed. It is of interest to note that to achieve proper exposure the intensity of the light had to be reduced by a factor of 800. The shock waves that appear here are visible due to the Schlieren effect where the refracted rays simply missed the camera lens. This indicates the possibilities of the laser when used as a light

source in a standard Schlieren setup.

Figure 30 shows the collapse of bubbles generated in water by means of a magnetostrictive horn. This collapse is evidenced mainly by the shock waves that are generated; as the details of the extremely small individual bubbles are not clearly visible. The quality of this print, as well as some of the previous ones, is somewhat poorer than the original due to the reduction in size necessary.

The major drawback in the use of a laser for photography is the structure of the light as may be seen in Fig. 30. It is felt that this is partially due to deterioration of the ruby as it was not nearly so pronounced in earlier pictures. The problem is most critical when low magnification pictures are desired. Fortunately, in this case the intensity of the light is much higher than required. Therefore a diffuser may be used to make the background more uniform, if the collimated nature of the light is not required. An alternate method which is presently under investigation is the use of optical fibers with randomly oriented fibers.

In addition to the rather broad areas of photography discussed thus far, the laser when operating in the pulsed mode has several other interesting applications. One of the most intriguing ones is the use of a series of pulses for optical ranging radar in space vehicles. The accuracy in control of the frequency of the pulse train in conjunction with the sharp front on each individual pulse suggests that a high degree of precision could be achieved in such an application.

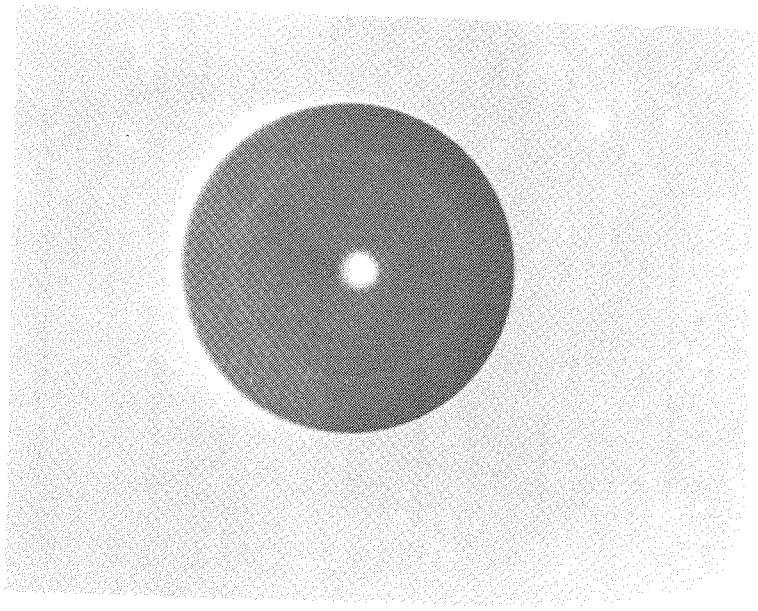

(a)

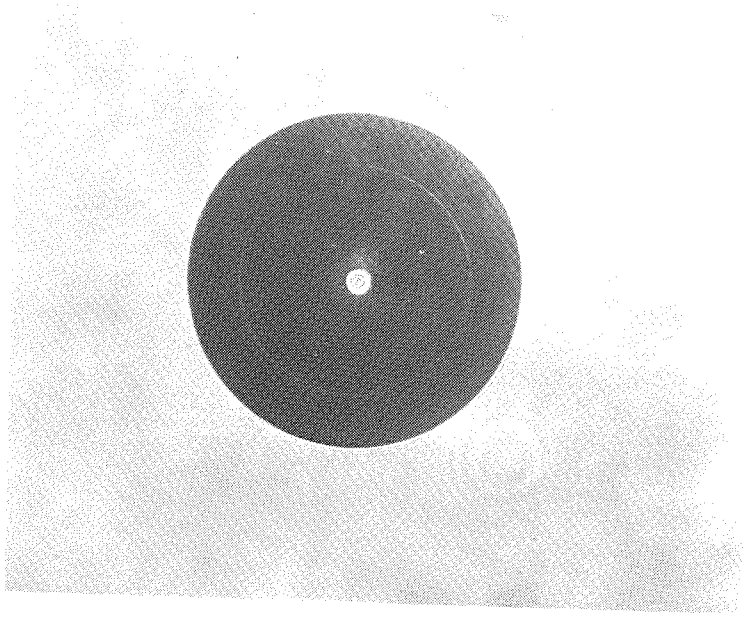

(b)

Fig. 24. An air bubble photographed in silhouette; (a) using a high pressure mercury arc lamp, (b) using a laser. The bubble is held stationary by an acoustical field (diameter of bubble is 0.13 cm).

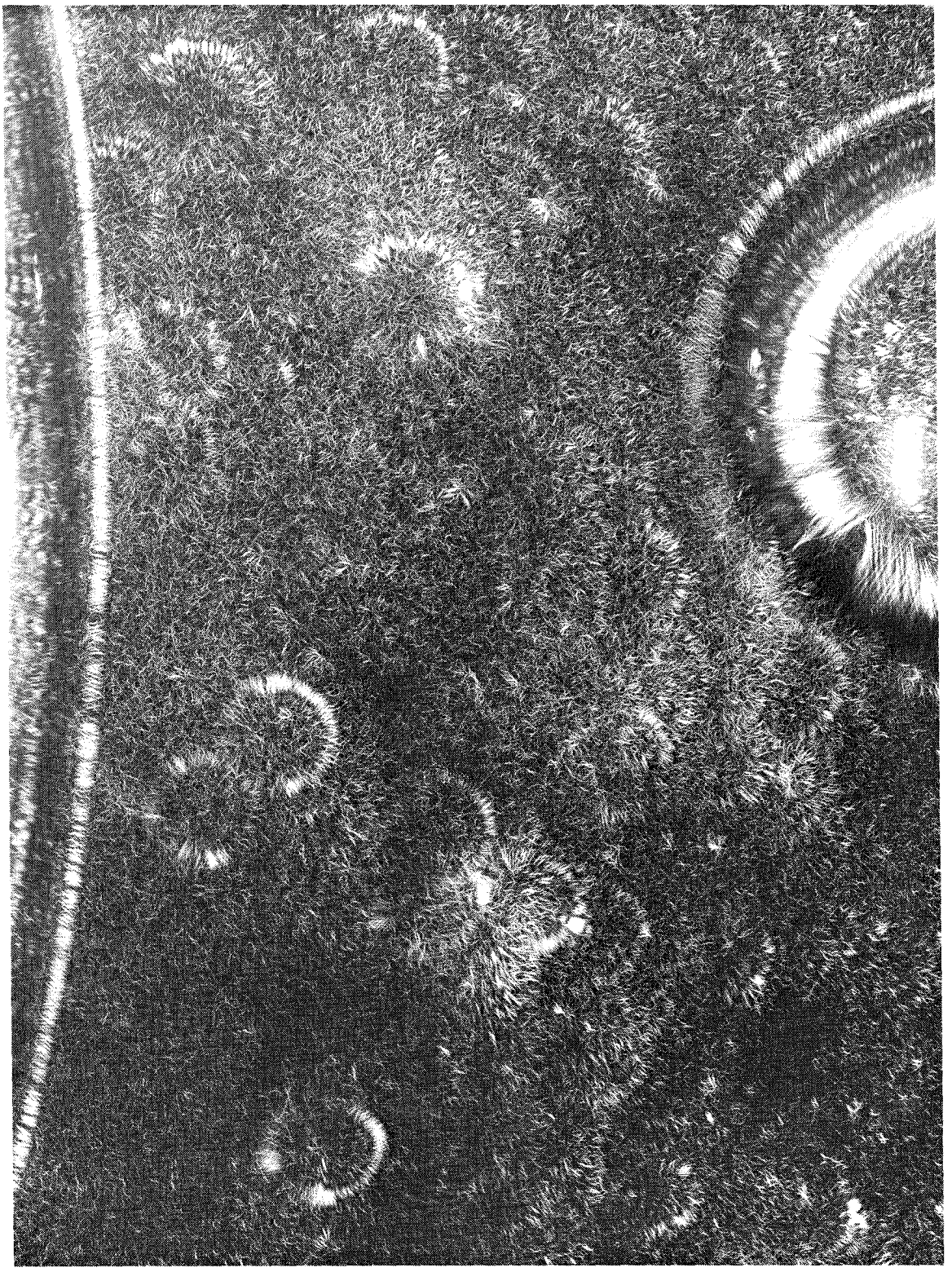

Fig. 25. Photograph by forward scattered light of a concentrated solution of polystyrene spheres (0.285 microns in diameter) in water. The picture was taken at a linear magnification of 50.

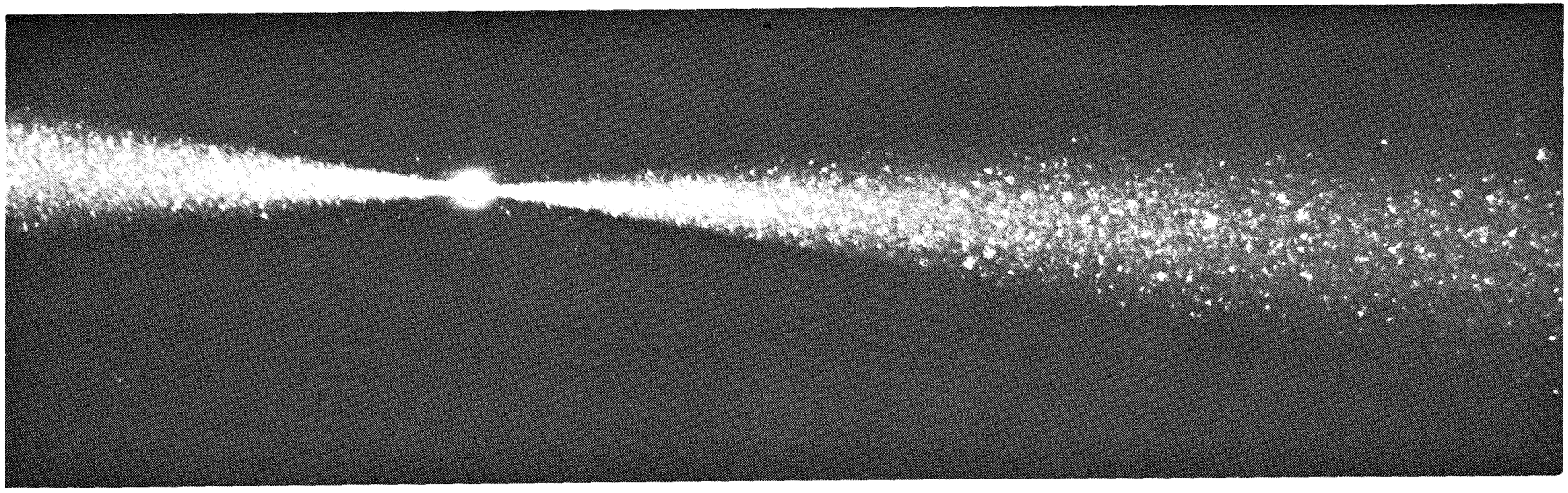

Fig. 26. Vapor bubbles generated in water by means of a focused laser beam.

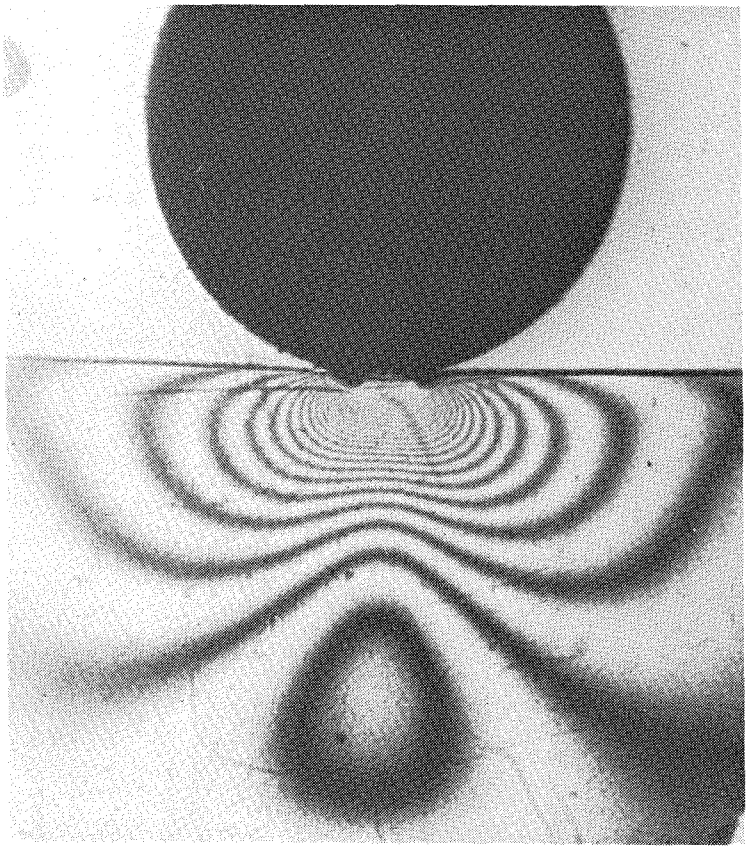

Fig. 27. Photoelastic picture of a specimen subjected to a concentrated load.

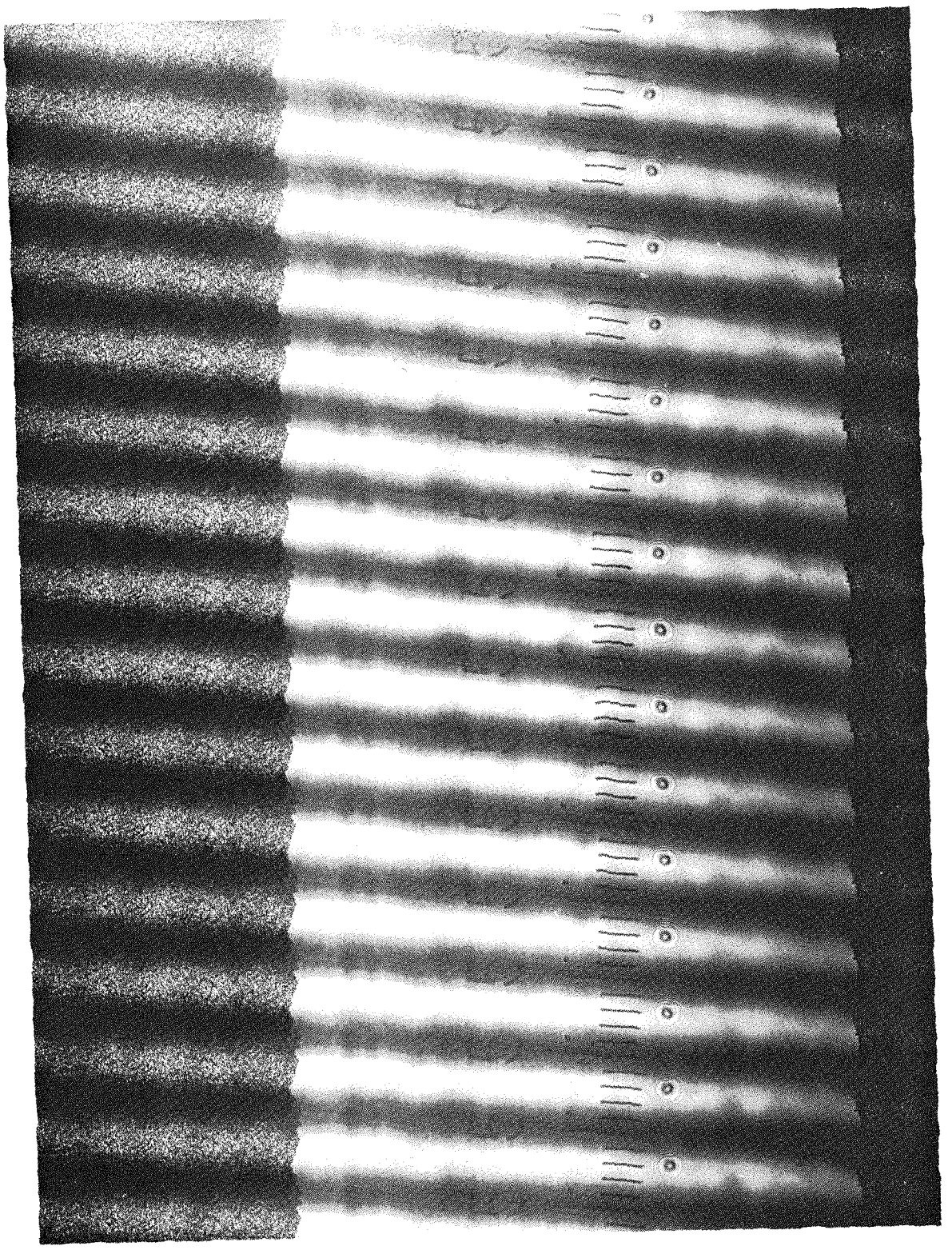

Fig. 28. Ground-glass microscope scale, shown at a magnification of 25. Picture taken at 2×10^5 frames per second and an exposure time of 30 nsec.

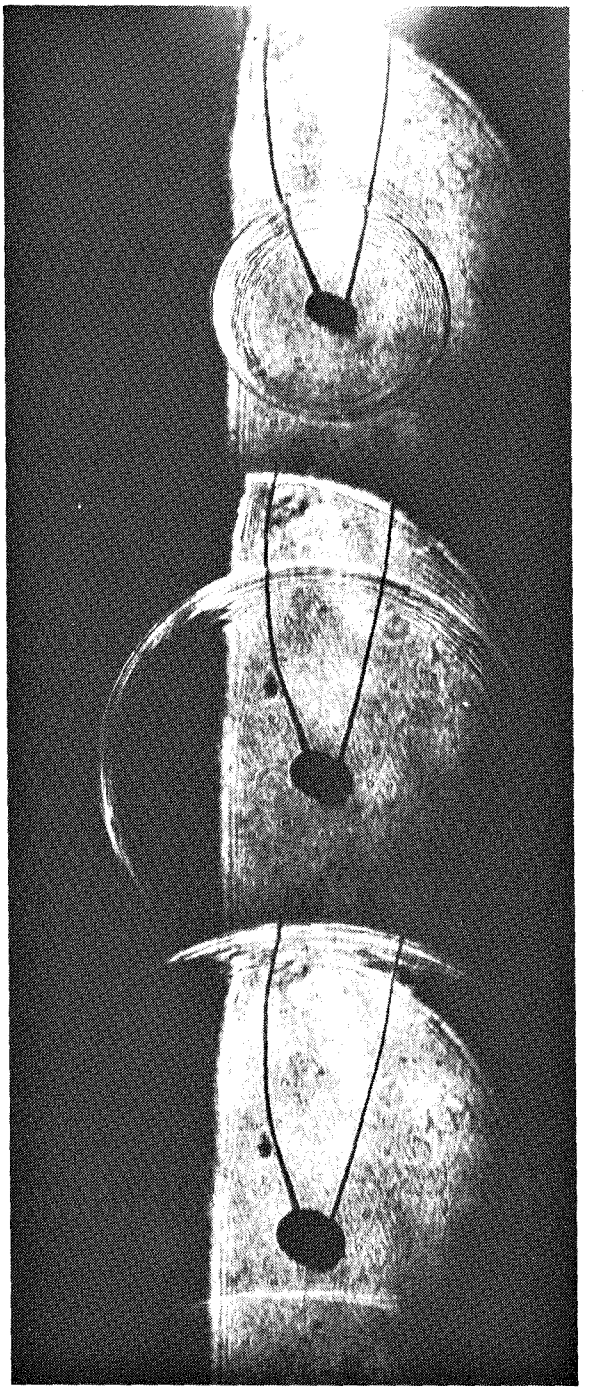

Fig. 29. Generation of a bubble in water by means of an electrical discharge.

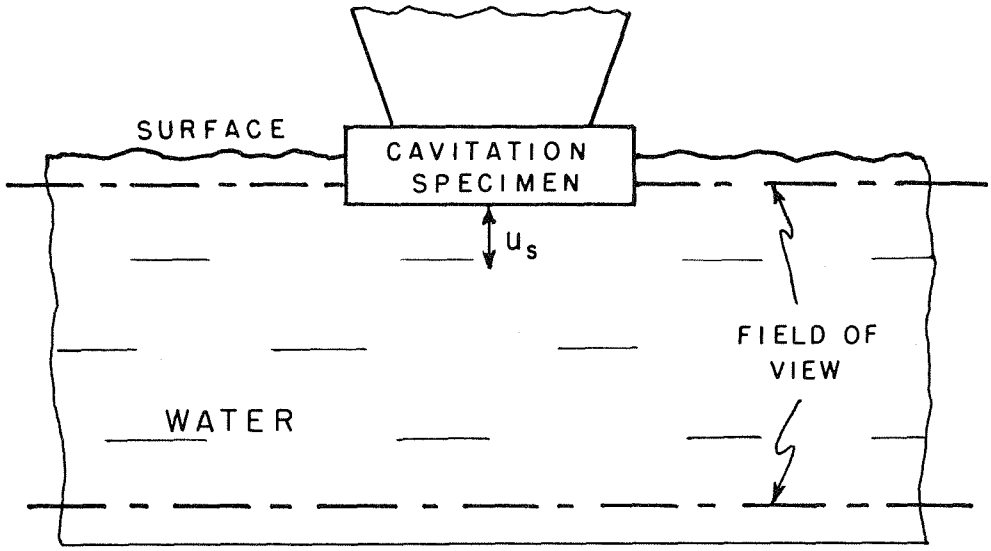

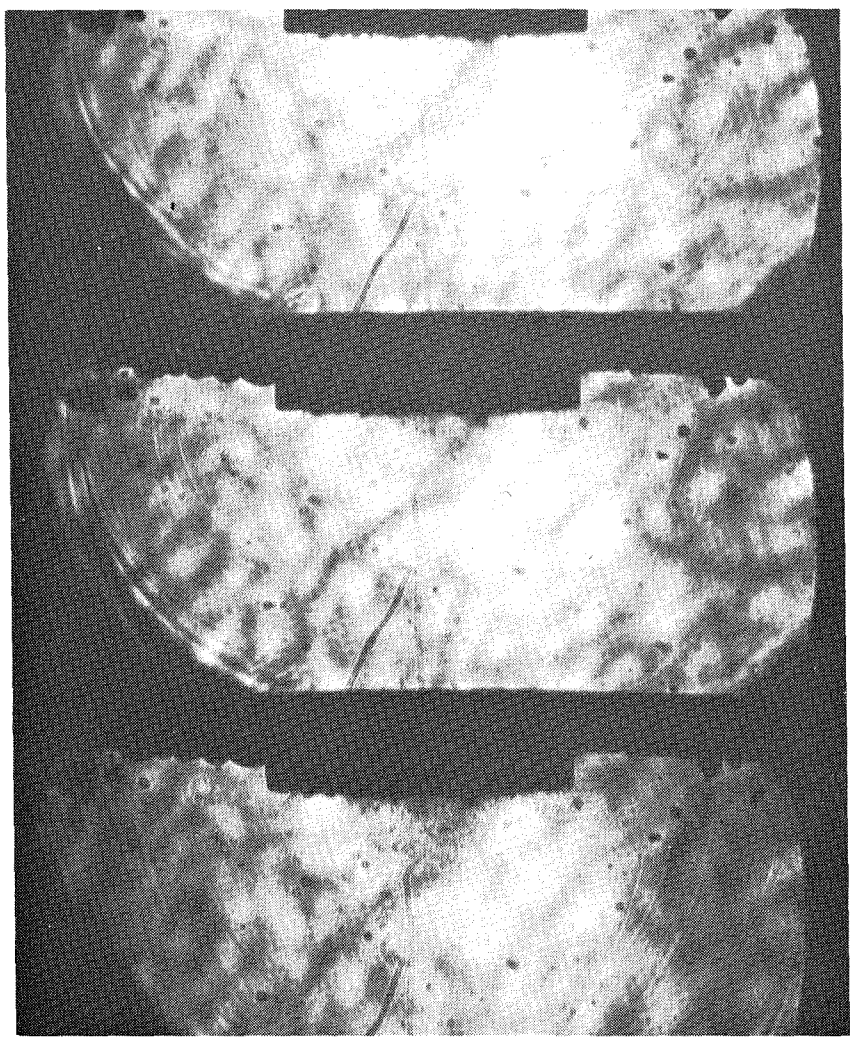

Fig. 30. Cavitation damage test specimen. Driven by magnetostrictive horn at 10kc/sec. u_s indicates the harmonic surface displacement.

SECTION E: CONCLUSIONS

The conclusions of this investigation may be summarized as follows:

(a) The laser is an exceedingly useful tool in areas of research involving photographic techniques.

(b) When a Kerr cell is used as a Q spoiling device, the laser may be pulsed repetitively at rates greater than 1.3 Mc.

(c) The pulse train generated in this fashion achieves a stabilized amplitude above a certain critical repetition rate.

(d) This critical repetition rate is found to be a function of the cavity length.

(e) The amplitude of this stabilized pulse train is a function of repetition rate and cavity length. This variation has been determined and is shown in Fig. 17. An explanation as to the phenomena which are responsible for this variation is given in section B.

(f) The duration of each individual pulse is 30 nsec for the laser used in this investigation, and is found to be independent of repetition rate. In a ruby laser, this pulse duration is determined to be a function of the pumping power.

(g) High speed photography using a laser at rates of over 1.3 million frames per second and exposure time of 30 nanoseconds has been achieved. The intensity of the light makes it possible to take pictures at these rates and at a magnification of 50.

(h) The definition achieved using a laser exceeds that possible using conventional light sources.

As stated in the introduction, the field is lasers is a new and rapidly expanding one. Applications are as varied as the problems which must be solved.

REFERENCES

1. A. L. Schawlow and C. H. Townes, Infrared and optical maser, Phys. Rev., 112, 1940, (1958).

2. T. H. Maiman, Optical and microwave optical experiments in ruby, Phys. Rev. Letters, 4, 564, (1960).

3. C. H. Townes, Quantum Electronics, Columbia University Press, New York, (1960).

4. J. R. Singer, Advances in Quantum Electronics, Columbia University Press, New York, (1961).

5. Bela A. Lengyel, Lasers, John Wiley and Sons, Inc., New York, (1962).

6. Quantum Electronics, Proceeding of the IEEE, Vol. 51, No. 1, 1-294, Jan., (1963).

7. Applied Optics, Vol. 1, No. 5, Sept., (1962).

8. Masers and Lasers (a report bibliography), ASTIA, No. AD-271-100, Feb., (1962).

9. D. F. Nelson and R. J. Collins, The polarization of the output from a ruby optical maser, Advances in Quantum Electronics, Columbia University Press, New York, (1961).

10. E. C. Kembles, Fundamental Principles of Quantum Mechanics, McGraw-Hill Book Co., Inc., New York, (1937).

11. J. L. Powell and B. Crasemann, Quantum Mechanics, Addison - Wesley Publishing Co., Inc., Cambridge, Mass., (1961).

12. Albert K. Levine, Lasers, American Scientist, Vol. 51, No. 1, 14-31, Mar., (1963).

13. T. H. Maiman, Stimulated optical emission in fluorescent solids, I Theoretical considerations, Phys. Rev., 123, 1145-50, (1961).

14. T. H. Maiman, et al, Stimulated emission in fluorescent solids, II Spectroscopy and stimulated emission in ruby, Phys. Rev., 123, 1151-1157, (1961).

15. F. J. McClung and R. W. Hellwarth, Giant optical pulsations from ruby, J. Appl. Phys., 33, 828-829, Mar., (1962).

II. TORSIONAL MAGNETOELASTIC WAVES IN A CIRCULAR CYLINDER

ABSTRACT

In this paper the effect of an electromagnetic field on the propagation of a pure torsional elastic wave in a conducting circular cylinder is investigated. The general field equations and boundary conditions are linearized and the equations of motion for an infinitely long circular rod are obtained for the particular electromagnetic field configurations considered.

The torsional motion of a solid rod in a steady axial magnetic field with and without a steady electric field is considered. In the first case it is found that a pure torsional mode will not propagate. In the second case a pure torsional mode will propagate and its frequency equation is obtained. The results for a perfect conductor are compared to a real material.

The torsional motion of a hollow rod in a steady tangential magnetic field with and without a steady axial electric field is considered. Without the electric field the equations are completely uncoupled and the solution is the standard elastic one. The electric field introduces coupling via the induced magnetic field. The equations of motion are obtained, however the actual solutions are not obtained due to the mathematical complexity involved.

TABLE OF CONTENTS

Part II

LIST OF SYMBOLS

B ~ magnetic flux density

D ~ dielectric displacement

E ~ electric field intensity

H ~ magnetic field intensity

j ~ current density

u ~ particle displacement

v_m ~ magnetic velocity = $(\mu H_z/\rho)^{\frac{1}{2}}$

v_s ~ shear velocity = $(G/\rho)^{\frac{1}{2}}$

ϵ ~ inductive capacity

λ, G ~ Lame constants for an elastic solid

μ ~ magnetic permeability

ρ ~ material density

ρ_e ~ charge density

σ ~ conductivity

τ ~ skin depth; $1/\tau^2 = \sigma\omega\mu$

ω ~ frequency of torsional wave

SECTION A: INTRODUCTION AND STATEMENT OF PROBLEM

I. Introduction

In the past few years a considerable amount of research has been focused on extensions of dynamical theories of continuous media to cases where a magnetic field is present. The subject of magnetohydrodynamics is the most notable of these with an extensive research program now in progress. The field of magnetoelasticity had received little attention until 1956 and even now is not nearly as well studied as magnetohydrodynamics.

The early studies in magnetoelasticity were conducted by Knopoff [1], Chadwick [2], and Kaliski [3, 4, 5]. The motivation for the first two was to determine the effect of the terrestrial magnetic field on seismic waves. The results of these studies were to conclude that the effect was too small to be of importance in this area. On the other hand Kaliski viewed the problem as one in applied mathematics and proceeded to work out the equations of motion in general for an elastic and inelastic anisotropic solid. The majority of this work was for a perfectly conducting infinite solid with the exception of reference (5) which is concerned with Rayleigh waves in a half space. Percival [6] and Miles [7] concerned themselves with a thin shell in a magnetic field. Dunkin and Eringen's [8] study was quite similar in approach to that of Chadwick except that they included the effect of an electric field as well as a magnetic one. Also, in addition to considering an infinite medium, they solved the problem of a limited class of vibrations of an infinite flat plate.

The sole experimental investigation that appears in the literature was by Winnett [9], who considered the longitudinal vibration of a circular rod. His results were in fair agreement with the linearized theory and his experiment pointed out the difficulty in obtaining an accurate measurement of such a small effect.

In general most of the previous investigations were made either for a perfect conductor or an infinite medium, or both. The

purpose of the present investigation was to include the effects of both finite conductivity and the boundary for one particular geometry. Therefore an effort was made to select a problem for which the elastic solution would be quite simple. The torsional problem of a circular cylinder was chosen. The investigation was further limited to pure torsional waves in an infinite rod.

The scope of the investigation was to obtain the equations of motion for the configurations selected and to investigate the coupling of the elastic waves and the electromagnetic fields. An underlying aim of this investigation was to choose the configuration most suitable for an experimental investigation. The approach presented is similar to that of Chadwick and Dunkin and Eringen, but differs from that of Knopoff and Miles.

II. General Equations and Boundary Conditions

In the problem of magnetoelasticity the coupling between an elastic wave propagating through a conducting medium and an electromagnetic field is studied. The equations governing the electromagnetic fields are the well known Maxwell's equations:

$$\nabla \times \vec{H} = \vec{j} + \frac{\partial \vec{D}}{\partial t} \qquad (1)$$

$$\nabla \times \vec{E} + \mu \frac{\partial \vec{H}}{\partial t} = 0 \qquad (2)$$

$$\nabla \cdot \vec{H} = 0 \qquad (3)$$

$$\nabla \cdot \vec{D} = \rho_e \qquad (4)$$

where $\vec{D}$ is the dielectric displacement and $\vec{H}$ is the magnetic field intensity and these quantities are related to the electric field intensity and the magnetic flux density by the following relation

$$\vec{B} = \mu \vec{H}, \qquad \vec{E} = \frac{1}{\epsilon} \vec{D}$$

μ is the magnetic permeability and ϵ the inductive capacity. The current equation for a linear isotropic conductor is:

$$\vec{j} = \sigma(\vec{E} + \vec{v} \times \mu \vec{H}) + \rho_e \vec{v} \qquad (5)$$

where σ is the conductivity, ρ_e the static charge density and $\vec{v}$ the particle velocity.

The equation of motion for a linear elastic solid with the electromagnetic force included is:

$$\rho \frac{\partial^2 \vec{u}}{\partial t^2} = (\lambda + G) \nabla (\operatorname{div} \vec{u}) + G \nabla^2 \vec{u} + \vec{j} \times \mu \vec{H} + \rho_e \vec{H} \qquad (6)$$

where λ and G are the Lamé constants for an elastic solid and ρ is the material density.

The system of units used is the m.k.s., or Giorgi system which is defined by Stratton [14]. This system appears to be accepted by most engineers and physicists although universal agreement certainly does not exist. The selection of a system of units is somewhat more important when two dynamical theories are combined.

The general electromagnetic boundary conditions for a moving medium are obtained in reference (8) and are summarized here. The boundary is shown in Fig. 1 with the system of unit vectors which will be used. The tangential boundary conditions are:

$$\left|\left[\vec{E} + \vec{v} \times \vec{B}\right]\right|_t = 0 \qquad (7)$$

$$\left|\left[\vec{H} - \vec{v} \times \vec{D}\right]\right|_t = \mathcal{L}_m^s - \rho^s v_m \qquad (8)$$

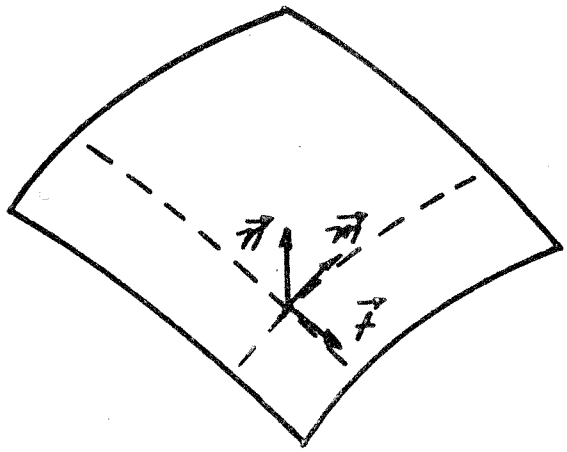

Figure (1): Boundary and system of coordinates.

where the subscripts m, n, and t refer to the unit vectors, the superscript s refers to a surface quantity and the symbol $\left|\left[A\right]\right|_t$ means the difference in the tangential component of A across the boundary. The conditions on the field components normal to the boundary are:

$$\left|\left[\vec{B}\right]\right|_n = 0 \qquad (9)$$

$$\left|\left[\vec{D}\right]\right|_n = \rho^s \qquad (10)$$

In most cases the normal component of the current must be continuous, hence

$$\left|\left[\sigma(\vec{E} + \vec{v}\times\vec{B})\right]\right|_n = 0 \qquad (11)$$

also serves as a normal boundary condition. If the boundary is between a solid medium and free space the velocity in all cases is that of the surface of the solid. The elastic boundary conditions are those of linear elastic theory.

III. Restricted Equations and Boundary Conditions

In general the total magnetic and electric fields will consist of a large statically applied field plus a small fluctuating part. Thus the total fields are given by:

$$\vec{H} = \vec{H}_0 + \vec{h} \qquad (12)$$

$$\vec{E} = \vec{E}_0 + \vec{e} \qquad (13)$$

These are inserted into equations (1) through (6) a system of nonlinear equations arises. To be consistent with linear elastic theory these equations are linearized by neglecting terms containing products of the small fluctuating quantities, such as $\vec{v}\times\vec{h}$, $\vec{j}\times\vec{h}$, etc. In addition we note that the elastic wave velocities are such that they are small compared to the propagation velocity of any electromagnetic quantities. Hence we ignore displacement currents, which is accomplished by dropping the last term in equation (1). Also the rod to be investigated will be infinite in length and initially without static charge density, therefore no charge density may be built up within the medium and ρ_e may be assumed to vanish. Therefore the governing equations now become:

$$\nabla \times \vec{H} = \vec{j} \qquad (14)$$

$$\nabla \times \vec{E} + \mu \frac{\partial \vec{H}}{\partial t} = 0 \qquad (15)$$

$$\vec{j} = \sigma (\vec{E} + \vec{v} \times \mu \vec{H}_0) \qquad (16)$$

$$\rho \frac{\partial^2 \vec{u}}{\partial t^2} = (\lambda + G) \nabla (\operatorname{div} \vec{u}) + G \nabla^2 \vec{u} + \vec{j} \times \mu \vec{H}_0 \qquad (17)$$

with the conditions that the electric and magnetic fields must have zero divergence.

In the linearization of the boundary condition the surface currents are assumed to vanish so that equations (7) through (11) become

$$\left| [\vec{E} + \mu \vec{v} \times \vec{H}_0] \right|_t = 0 \qquad (18)$$

$$\left| [\vec{H}_0 + \vec{h}] \right|_t = 0 \qquad (19)$$

$$\left| [\mu (\vec{H}_0 + \vec{h})] \right|_n = 0 \qquad (20)$$

$$(\vec{E} + \mu \vec{v} \times \vec{H}_0)_n = 0 \qquad (21)$$

$$\left| [\epsilon \vec{E} + \mu \vec{v} \times \vec{H}_0] \right|_n = \rho_e^s \qquad (22)$$

where the last condition merely defines the surface charge and results from equation (10) with

$$\vec{D} = \epsilon \vec{E} + \delta \vec{v} \times \vec{H} \qquad (23)$$

where

$$\delta = \epsilon\mu - \epsilon_0\mu_0 \qquad (24)$$

with the subscript o referring to the quantities in free space. The last term in equation (23) results from consideration of electromagnetic theory of a moving medium.*

If these equations are to hold when the small fluctuating fields vanish then H_o and E_o must automatically satisfy their jump conditions, i.e.

$$|[H_o]|_t = 0 \ , \quad \text{etc.}$$

Hence equations (18) through (22) reduce to

$$|[\vec{e} + \mu \vec{v} \times \vec{H}_o]|_t = |[\vec{h}]|_t = |[\mu \vec{h}]|_n$$
$$= (\vec{e} + \mu \vec{v} \times H_o)_n = 0 \qquad (25)$$

and

$$\rho_e^s = |[\epsilon \vec{e}]|_n + \delta (\vec{v} \times \vec{H}_o)_n \qquad (26)$$

---

* Practically speaking $\alpha \approx 0$ and is included here only for the sake of completeness. This then becomes equivalent to the definition of the dielectric displacement given on page (59).

Since the charge density within the body is zero the current equation (16) reduces these to:

$$\left.\begin{aligned} \left|\left[\vec{h}\right]\right|_t &= \left|\left[\mu \vec{h}\right]\right|_n = 0 \\ \left|\left[\dot{\vec{\sigma}} \vec{E}\right]\right|_t &= (\dot{E})_n = 0 \end{aligned}\right\} \qquad (27)$$

which are the linearized boundary conditions.

IV. Statement of Problem

The propagation of pure torsional waves in a circular cylinder under the influence of an electromagnetic field is to be studied. The rod is taken to be infinite in length and the applied field constant in time, hence as stated previously no possibility exists for a build-up of static charge density within the medium. Also surface currents are ignored. Four cases are to be studied:

Axial magnetic field:

I. With an axial electric field.

II. With vanishing electric field.

Tangential magnetic field:

III. With no electric field.

IV. With an axial electric field.

In cases I and II the applied magnetic field would be obtained from a solenoid of infinite length, hence the field is constant. The electric field is obtained by passing a steady state current through the rod. This electric field then induces a tangential magnetic field which must be considered. The rod in these two cases is solid and of radius b. The current density of the steady electric field is assumed uniform

In the third and fourth cases the applied magnetic field would be obtained by passing current down the outer conductor of a co-

axial conductor and back along the center. This would necessitate a hollow rod and result in a magnetic field that varies as $1/r$. The electric field would again be generated by passing a current along the rod and as before this would induce an additional tangential magnetic field.

Since this investigation is limited to pure torsional waves the displacement field of the rod is specified to contain only a tangential component, i.e. u_θ is the only nonvanishing component. This may be a function of the radial coordinate r, and the axial coordinate z, but the symmetry in the θ coordinate rules out any dependence on this variable. This places rather strict restrictions on the modes that may be studied; however, it is felt that this method of approach will be more fruitful than a direct attack on the general problem which might well prove unmanageable in the end.

In general even though the equations have been linearized they are still a system of partial differential equations, the straightforward solution to which might prove a formidable task. Hence a product solution with harmonic variation in time will be sought. This reduces the governing equations to a system of linear ordinary differential equations. In particular, the small fluctuating quantities such as $\vec{j}$, $\vec{h}$, $\vec{u}$, etc., will be assumed to be propagating in the z, or axial direction with harmonic time dependence. Therefore a general quantity will have the form

$$\phi(r, z, t) = \phi(r)\, e^{i(\omega t - \gamma z)} \qquad (28)$$

where we choose to study the case of the frequency ω real and the propagation paramenter γ may in general be complex. This approach was chosen by Chadwick [2] and others [8]; however, several authors [1, 7, 9] have chosen the alternate approach of complex frequency.

SECTION B: AXIAL MAGNETIC FIELD

I. Case I: Axial Magnetic Field with Axial Electric Field

The geometry and coordinate system to be used are shown in Fig. 2. The applied fields H_z and E_z are constant and the tangential magnetic field induced by the electric field is given by:

$$\left.\begin{aligned} H_\theta &= \frac{\sigma b^2}{2r} E_z && \text{outside} \\ H_\theta &= \frac{\sigma r}{2} E_z && \text{inside} \end{aligned}\right\} \quad (31)$$

Hence the applied fields within the rod are:

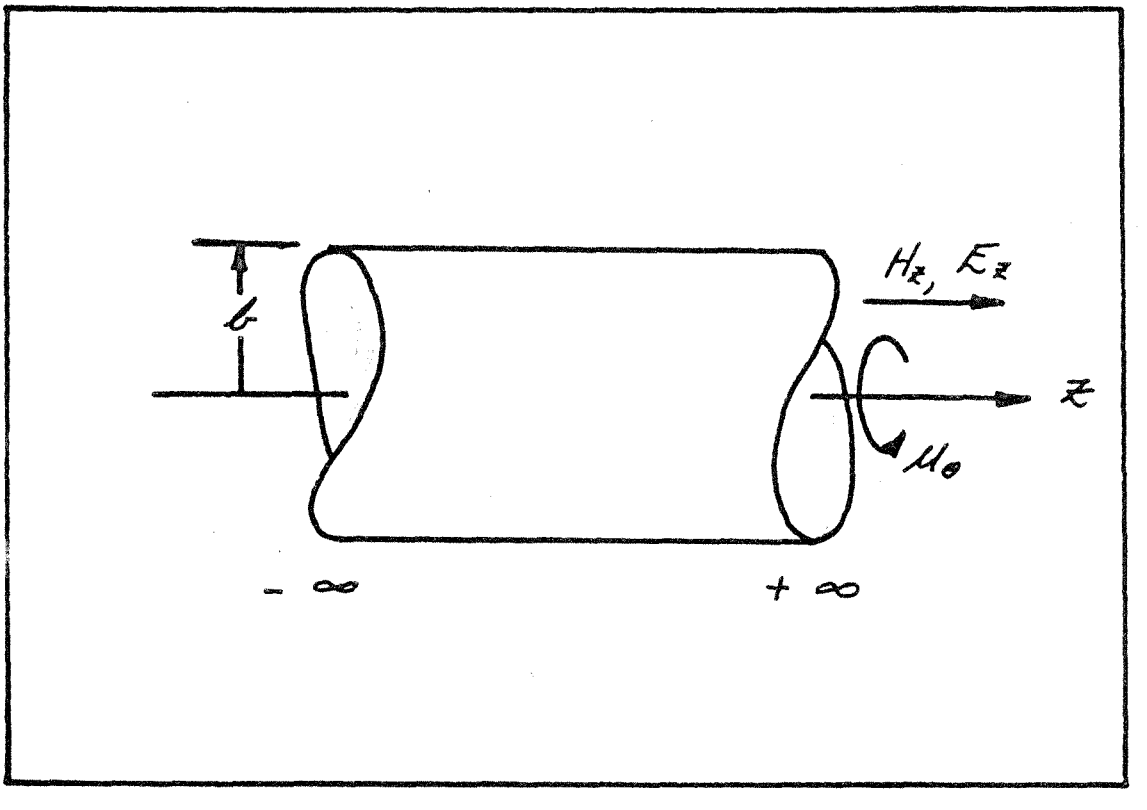

Fig. 2. Solid rod with axial magnetic and electric fields.

$$\vec{H_0} = H_z \hat{i}_r + \frac{\sigma r}{2} E_z \hat{i}_\theta \qquad (32)$$

$$\vec{E_0} = E_z \hat{i}_z \qquad (33)$$

where $\hat{i}_r$, $\hat{i}_z$ and $\hat{i}_e$ are the unit vectors.

In addition the current must also have a static z-component:

$$\vec{j_T} = \sigma E_z \hat{i}_z + \vec{j} \qquad (34)$$

where j_T is the total current and $\vec{j}$ represents the fluctuating current.

If equations (32) through (34) plus the assumed displacement field are introduced into the governing equations (14) through (17), and equation (28) is utilized the equations may be written out in component form as follows:

$$\left.\begin{aligned} & i\gamma h_\theta - j_r = 0 \\ & -i\gamma h_r - \frac{dh_z}{dr} - j_\theta = 0 \\ & \tfrac{1}{r}\frac{d}{dr}(r h_\theta) - j_z = 0 \end{aligned}\right\} \qquad (35)$$

$$\left.\begin{aligned} & i\gamma e_\theta + i\omega\mu h_r = 0 \\ & -i\gamma e_r - \frac{de_z}{dr} + i\omega\mu h_\theta = 0 \\ & \tfrac{1}{r}\frac{d}{dr}(r e_\theta) + i\omega\mu h_z = 0 \end{aligned}\right\} \qquad (36)$$

$$\left.\begin{aligned} & j_r = \sigma(e_r + i\omega\mu H_z u_\theta) \\ & j_\theta = \sigma e_\theta \\ & j_z = \sigma e_z \end{aligned}\right\} \qquad (37)$$

$$\left.\begin{aligned} & \mu\left[H_z j_\theta - \frac{\sigma r}{2} E_z j_z - \sigma E_z h_\theta - \frac{\sigma^2 E_z^2 r}{2}\right] = 0 \\ & G\left[\nabla^2 u_\theta - \tfrac{1}{r^2} u_\theta\right] + \rho\omega^2 u_\theta + \mu\left[\sigma E_z h_r - H_z j_r\right] = 0 \\ & \tfrac{1}{2}\mu\sigma E_z r j_r = 0 \end{aligned}\right\} \qquad (38)$$

From the third equation or z component of (38) for a non-vanishing electric field it is evident that j_r must vanish. This condition naturally arises from the assumed displacement field of a pure torsional wave, that is, $u_z = 0$. From equation (35-r) this condition also implies that h_θ must be zero, this in turn through equation (35-z) implies that j_z must vanish. Finally the condition is reached where all of the induced quantities must vanish in order that the equations remain consistant. Hence we conclude that a pure torsional wave cannot propagate under the specified arrangement of fields.

II. Case II: Vanishing Electric Field

The other alternative left in equation (38-z) is to assume that the electric field vanishes, which is the condition specified for case II. Under this assumptions the equations become:

$$\left.\begin{aligned} i\gamma h_\theta - j_r &= 0 \\ -i\gamma h_r - \frac{dh_z}{dr} - j_\theta &= 0 \\ \tfrac{1}{r}\frac{d}{dr}(r h_\theta) - j_z &= 0 \end{aligned}\right\} \qquad (35')$$

$$\left.\begin{aligned} i\gamma e_\theta + i\omega\mu h_r &= 0 \\ -i\gamma e_r - \frac{de_z}{dr} + i\omega\mu h_\theta &= 0 \\ \tfrac{1}{r}\frac{d}{dr}(r e_\theta) + i\omega\mu h_z &= 0 \end{aligned}\right\} \qquad (36')$$

$$\left.\begin{aligned} j_r &= \sigma(e_r + i\omega\mu H_z u_\theta) \\ j_\theta &= \sigma e_\theta \\ j_z &= \sigma e_z \end{aligned}\right\} \qquad (37')$$

$$\left.\begin{aligned} \mu H_z j_\theta &= 0 \\ G[\nabla^2 u_\theta - \tfrac{1}{r^2}u_\theta] + \rho\omega^2 u_\theta - \mu H_z j_r &= 0 \\ 0 &= 0 \end{aligned}\right\} \qquad (38')$$

In equation (38'-r) if the magnetic field does not vanish, then $j_\theta = 0$, which leads through the remainder of the equations to the following conditions:

$$u_r = 0 \qquad j_r \qquad h_r = 0 \qquad e_r$$
$$u_\theta \qquad j_\theta = 0 \qquad h_\theta \qquad e_\theta = 0$$
$$u_z = 0 \qquad j_z \qquad h_z = 0 \qquad e_z$$

and the remaining equations are:

$$\left.\begin{aligned} ir h_\theta - j_r &= 0 \\ \tfrac{1}{r}\frac{d}{dr}(r h_\theta) - j_z &= 0 \end{aligned}\right\} \quad (35')$$

$$ir e_r - \frac{de_z}{dr} + i\omega\mu h_\theta = 0 \qquad (36')$$

$$\left.\begin{aligned} j_r &= \sigma(e_r + i\omega\mu H_z u_\theta) \\ j_z &= \sigma e_z \end{aligned}\right\} \quad (37')$$

$$G[\nabla^2 u_\theta - \tfrac{1}{r^2}u_\theta] + \rho\omega^2 u_\theta - \mu H_z j_r = 0 \qquad (38')$$

If the remaining components of the magnetic field and electric field are eliminated as well as j_z, these equations may be reduced to the two equations

$$\nabla^2 u_\theta - \tfrac{1}{r^2}u_\theta + \frac{\rho\omega^2}{G}u_\theta - \frac{\mu H_z}{G} j_r = 0 \qquad (39)$$

$$\frac{d}{dr}\left(\tfrac{1}{r}\frac{d}{dr}(r j_r)\right) - \gamma^2 j_r - i\omega\mu\sigma j_r + ir^2\omega\mu\sigma H_z u_\theta = 0 \qquad (40)$$

which is a system of coupled second order, linear ordinary differential equations with non-constant coefficients. We also note that the two differential operators:

$$\nabla^2\phi - \tfrac{1}{r^2}\phi = \frac{d^2\phi}{dr^2} + \tfrac{1}{r}\frac{d\phi}{dr} - \gamma^2\phi - \tfrac{1}{r^2}\phi$$

and

$$\frac{d}{d\eta}\left(\frac{1}{\eta}\frac{d}{d\eta}(\eta\phi)\right) - \gamma^2\phi = \frac{d^2\phi}{d\eta^2} + \frac{1}{\eta}\frac{d\phi}{d\eta} - \gamma^2\phi - \frac{1}{\eta^2}\phi$$

are equivalent and hence denote it as

$$L\phi = \frac{d^2\phi}{d\eta^2} + \frac{1}{\eta}\frac{d\phi}{d\eta} - \gamma^2\phi - \frac{1}{\eta^2}\phi \qquad (41)$$

Therefore the above equations may be rewritten in the form

$$L u_\theta + \left(\frac{\omega}{v_s}\right)^2 u_\theta - \frac{1}{H_z}\left(\frac{v_M}{v_s}\right)^2 j_1' = 0 \qquad (42)$$

$$L j_1' - i\frac{1}{\delta^2} j_1' + i\left(\frac{\gamma}{2}\right)^2 H_z u_\theta = 0 \qquad (43)$$

where

$$\frac{1}{\delta^2} = \sigma\omega\mu \qquad (44)$$

$$v_s^2 = G/\rho \qquad (45)$$

$$v_M^2 = \frac{\mu H_z^2}{\rho} \qquad (46)$$

Equation (44) defines the "skin depth" of a conductor in an electromagnetic field; (45) the shear velocity of an elastic wave, and (46) a magnetic velocity. The latter may be shown to correspond to the Alfven wave speed in a fluid. It is also of interest to note that the electromagnetic energy density in this case is given by

$$U = \frac{1}{2}\frac{B^2}{\mu} = \frac{1}{2}\mu H^2$$

if the small contribution due to the fluctuating fields is ignored.

Hence v_m^2 is the ratio of twice the electromagnetic energy density to the material density.

Now if the magnetic field vanishes in equation (42) it reduces to the elastic wave equation:

$$L u_0 + \left(\frac{\omega}{v_s}\right)^2 u_0 = 0 \qquad (47)$$

which has the solution

$$u_0 = A J_1(\lambda_1 r) + B Y_1(\lambda_1 r) \qquad (48)$$

with

$$\lambda_1^2 = \gamma^2 - \left(\omega/v_s\right)^2$$

where $J_1(\lambda_1 r)$ and $Y_1(\lambda_1 r)$ are Bessel functions of the first and second kind of the first order.

Likewise, equation (43) reduces to

$$L j_n - i \frac{1}{2} j_n = 0 \qquad (49)$$

which has the solution

$$j_n = C I_1(\lambda_2 r) + D K_1(\lambda_2 r) \qquad (50)$$

with

$$\lambda_2^2 = \gamma^2 + i \sigma \omega \mu$$

where $I_1(\lambda_2 r)$ and $K_1(\lambda_2 r)$ are the modified Bessel functions of the first and second kind and of the first order.

Hence we expect that, in general, equations (42) and (43) would have solutions of a similar form, that is, the entire character of the solutions would not be expected to change for a particular value

of the parameter H_z. (It is realized that this constitutes an assumption, the validity of which will be shown.)

Suppose the solution to equations (42) and (43) are some combination of Bessel Type functions. The only restriction that is placed on this function is that it obeys the Bessel function recursion relations:

$$\left.\begin{aligned} \frac{2\nu}{\chi} Z_\nu(\chi) &= Z_{\nu-1}(\chi) - Z_{\nu+1}(\chi) \\ 2 Z_\nu'(\chi) &= Z_{\nu-1}(\chi) + Z_{\nu+1}(\chi) \end{aligned}\right\} \qquad (51)$$

where $Z_\nu(\chi)$ is some Bessel Type function and the prime denotes differentiation with respect to the variable χ. It is shown[10] that this is true for linear combinations and products of both ordinary and modified Bessel functions. Therefore the form of the solutions is assumed to be:

$$\left.\begin{aligned} u_0 &= K_1 Z_1(\lambda_1 r) \\ j_r &= K_2 Z_1(\lambda_2 r) \end{aligned}\right\} \qquad (52)$$

Now, using the recursion relations (51),

$$L Z_1(\lambda_1 r) = -(\lambda_1^2 + \gamma^2) Z_1(\lambda_1 r) \qquad (53)$$

so that the system of differential equations may be reduced to the following system of algebraical ones:

$$\begin{pmatrix} -(\lambda_1^2+\gamma^2)+(\omega/v_s)^2 & -\frac{1}{H_z}(v_H/v_s)^2 \\ i(\gamma/c)^2 H_z & -(\lambda_2^2+\gamma^2)-i\frac{1}{c_2} \end{pmatrix} \begin{Bmatrix} K_1 Z_1(\lambda_1 \pi) \\ K_2 Z_1(\lambda_2 \pi) \end{Bmatrix} = \begin{Bmatrix} 0 \\ 0 \end{Bmatrix} \quad (54)$$

and the necessary and sufficient condition that a nontrivial solution exists is the vanishing of the determinant.

$$\begin{vmatrix} -(\lambda_1^2+\gamma^2)+(\omega/v_s)^2 & -\frac{1}{H_z}(v_H/v_s)^2 \\ -i(\gamma/c)^2 H_z & -(\lambda_2^2+\gamma^2)-i\frac{1}{c_2} \end{vmatrix} = 0 \quad (55)$$

This can be rewritten, using the knowledge that the elastic boundary conditions may be satisfied by setting $\lambda_1 = 0$, in the following form:

$$\gamma^4 + \left[\lambda_2^2 - (\omega/v_s)^2 + i\frac{1}{c_2}\left\{1 + (v_H/v_s)^2\right\}\right]\gamma^2 - \frac{1}{c_2}(\omega/v_s)^2 = 0 \quad (55)$$

This then constitutes the frequency equation for this case. The value of λ_2, as well as λ_1, are determined through the boundary conditions.

III. Restriction to a Perfect Conductor

The limiting case of a perfect conductor will be introduced as it results in some rather simple expressions for the wave speed and will provide a means of comparing these results with those presented in the literature. However, a word of caution must be

injected as, if a perfect conductor is assumed, this physically implies that the induced currents become large, thereby inducing large magnetic fields and the entire process of linearization may no longer be valid. With this possible restriction in mind equation (55) is rewritten by letting $\sigma \to \infty$, which implies $\tau \to 0$ in the following form:

$$\gamma^2 = \frac{(\omega/v_s)^2}{1+(v_H/v_s)^2} \qquad (56)$$

Since all quantities on the right hand side are real, $\gamma^2 = p^2$ and th velocity of propagation is given by

$$v_p^2 = v_s^2\left[1+(v_H/v_s)^2\right] \qquad (57)$$

and the damping coefficient β is zero. This is the same result tha Chadwick [2] obtained for a shear wave traveling in an infinite medium. Hence just as in the pure elastic case the torsional wave i a solid rod travels with the shear velocity and is neither damped nor dispersed.

IV. Boundary Conditions

If the finite conductivity is retained, the boundary conditions must be applied to obtain further information from equation (55). It may easily be shown that for this displacement field the only remaining elastic boundary condition of a stress free surface to be satisfied is:

$$\tau_{r\theta} = G\left\{r\frac{\partial}{\partial r}\left(\frac{u_\theta}{r}\right)\right\}\Big|_{r=b} = 0 \qquad (58)$$

If the form of assumed solution as given by equation (48) is retained, only the part containing $J_1(\lambda r)$ remains, since the condition of finite displacement at the center of the rod requires that the coefficient of $Y_1(\lambda r)$ vanishes. Hence equation (58) may be

written:

$$AG\lambda_1^2 \frac{d}{d(\lambda_1 r)}\left(\frac{J_1(\lambda_1 r)}{\lambda_1 r}\right)\Big|_{r=b} = 0 \qquad (58')$$

which may be satisfied by

$$\lambda_1 = 0 \qquad (59)$$

As in the elastic case, a possible solution for this value of λ_1 is

$$u_\theta = Ar \qquad (60)$$

which leaves equation (53) and hence (55) unchanged.

The boundary condition on the radial induced current is given by equation (27) as

$$j_r\Big|_{r=b} = 0 \qquad (61)$$

and, as in the displacement solution, only the $I_1(\lambda_2 r)$ term of equation (50) is retained. Therefore the boundary condition becomes:

$$I_1(\lambda_2 r)\Big|_{r=b} = 0 \qquad (61')$$

but $$I_1(\lambda_2 r) = -i J_1(i\lambda_2 r)$$

for

$$-\pi < \arg(\lambda_2 r) \leq \pi/2$$

$$\pi/2 < \arg(\lambda_2 r) \leq \pi$$

and equation (61') is:

$$J_1(i\lambda_2 b) = 0$$

The first root of this equation is the trivial one of zero which implies that the induced current vanishes. The next root is [13]:

$$i\lambda_2 b = 3.832 \qquad (62)$$

This corresponds to the lowest mode possible which is coupled to the electromagnetic fields and hence the first mode of interest. Selection of higher roots of equation (58') corresponds to modes that are highly damped and do not become important until the wavelength is much smaller than the radius of the rod. Likewise higher roots of equation (61') become important also under these conditions. These higher modes are equivalent to the second torsional mode in a solid elastic rod. The physical observation of this mode is extremely difficult.

V. A Numerical Example

For the purpose of illustrating the magnitude of the magnetoelastic effect a numerical example will be presented. Consider the following case which corresponds to an aluminum rod.

$$v_s = 3\times10^3 \text{ m/sec}$$
$$b = 1 \text{ cm}$$
$$\tfrac{1}{c^2} = \mu\sigma\omega = 40\omega$$
$$B = 10 \text{ webers/m}^2$$
$$\therefore \quad v_M^2 = 2.84\times10^4 \text{ m/sec}$$

and

$$(v_M/v_s)^2 = 4.39\times10^{-3}$$

First, the case of a perfect conductor will be considered. From equation (57) the change in the velocity of propagation is

$$v_\phi/v_s = 1 + 0.57 \times 10^{-3}$$

While this is capable of being measured experimentally a word of caution should be injected, namely that the assumed magnetic field is quite high and could only be obtained for a very short time. A more realistic value might be 1 weber/meter^2 which would yield

$$v_\phi/v_s = 1 + 0.57 \times 10^{-5}$$

the experimental measurement of which might justifiably be questioned.

Introduction of finite conductivity results in the velocity of propagation becoming a transcendental function of not only the magnetic field but also the frequency of the torsional wave. Therefore this mode will be dispersive as well as damped. This provides an excellent means of checking the theory by an experiment. If the same rod is considered and the numerical values are inserted into equation (55), the following results are obtained. Two values of γ^2 result; one corresponds to the mode of propagation that has been chosen for consideration; the other is a highly damped case with a very low velocity of propagation. For each of the γ^2 there are two roots which correspond to the righward and leftward traveling waves, hence the four roots of equation (55) are accounted for. The results of numerical calculation of the wave speed are shown in Fig. 3. It should be noted that these calculations involve taking the difference of large complex numbers which are approximately equal; therefore the values presented are for the purpose of showing the trend only. Upon first inspection the effect of the electromagnetic field seems quite large, however, this plot is for the phase velocity and the following must be considered. The signal, or information in a wave will be propagated with the group velocity which is given by

$$v_g = \frac{d\omega}{d\gamma}$$

Now if a plot of γ versus ω is made the group velocity may be determined. Upon investigation for this case the group velocity is found to be given by the shear velocity for frequencies at or above 100 kc and to fall off very rapidly to zero at approximately 50 kc. Therefore a lower limit on frequency is determined. Below this limit this mode will not propagate; most likely the pure elastic torsional wave would result. From 100 kc to 1 Mc the group as well as phase velocity is given by the shear velocity. Above 1 Mc the wavelength is shorter than the radius of the rod and higher modes would result. Hence if experiment measurements are to be made the range defined by Fig. 3 would be most useful. This type of behavior is quite similar to that found in waveguide problems.

In passing it is worthwhile noting that the experimental measurements of reference (9) were made in the range of frequencies defined by Fig. 3.

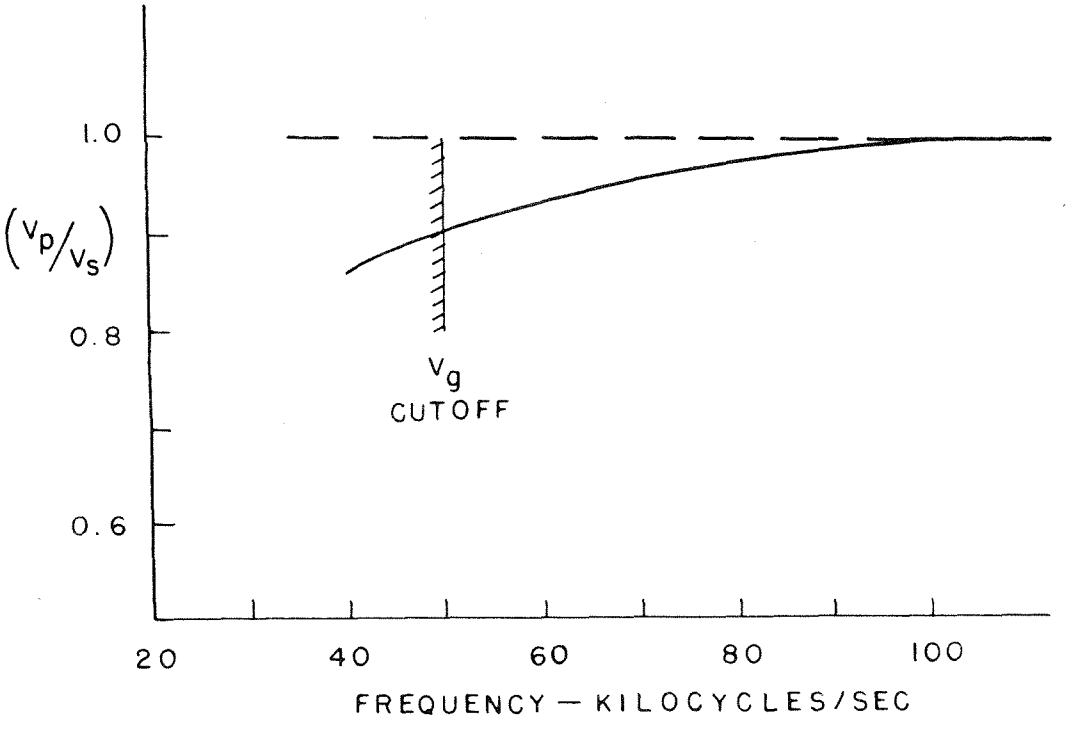

Fig. 3. Variation of phase velocity with frequency.

SECTION C: TANGENTIAL MAGNETIC FIELD

I. Case III: Magnetic Field Only

In the remaining two cases the applied magnetic field is tangential and is given by:

$$\vec{H_o} = \frac{I}{2\pi r}\,\hat{i_\theta} = \tfrac{1}{2} H_\theta\,\hat{i_\theta} \qquad (63)$$

where I is the total current being carried by the coaxial conductor which supplies the magnetic field.

The configuration to be considered and the coordinate system to be employed is shown in Fig. 4.

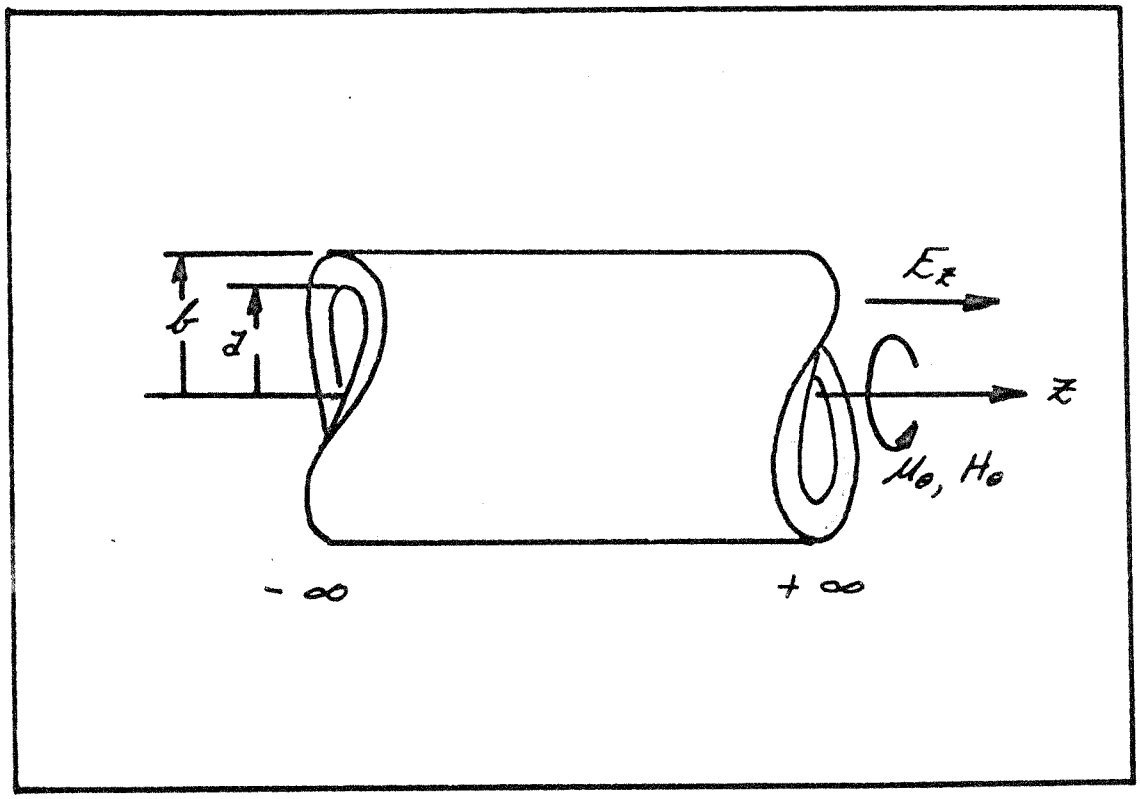

Fig. 4: Hollow rod with tangential magnetic field.

The governing equations are still given by equations (14) through (17) and the displacement field is completely specified by the tangential component u_θ. Upon substitution of this plus equation (63) into the governing equations, they become:

$$\left.\begin{aligned} i\gamma h_0 - j_{r_1} &= 0 \\ -i\gamma h_1 - \frac{dh_z}{dr} - j_{\theta_0} &= 0 \\ \tfrac{1}{r}\frac{d}{dr}(r h_0) - j_{z_1} &= 0 \end{aligned}\right\} \qquad (64)$$

$$\left.\begin{aligned} i\gamma e_0 + i\omega\mu h_1 &= 0 \\ -i\gamma e_1 - \frac{de_z}{dr} + i\omega\mu h_0 &= 0 \\ \tfrac{1}{r}\frac{d}{dr}(r e_0) + i\omega\mu h_z &= 0 \end{aligned}\right\} \qquad (65)$$

$$\vec{j} = \sigma\vec{e} \qquad (66)$$

$$\left.\begin{aligned} \tfrac{1}{r} H_0 j_{z_1} &= 0 \\ G[\nabla^2 u_0 - \tfrac{1}{r^2} u_0] + \rho\omega^2 u_0 &= 0 \\ \tfrac{1}{r} H_0 j_{r_1} &= 0 \end{aligned}\right\} \qquad (67)$$

The first and third equations of (67) imply that $j_r = j_z = 0$. This in turn through the remaining equations leads to the following conditions which must be satisfied in order that the equations will be consistent.

$u_{r_1} = 0$	h_{r_1}	$e_{r_1} = 0$	$j_{r_1} = 0$
u_{θ_0}	$h_{\theta_0} = 0$	e_{θ_0}	j_{θ_0}
$u_{z_1} = 0$	h_{z_1}	$e_{z_1} = 0$	$j_{z_1} = 0$

and the remaining equations are:

$$-i\gamma h_{r_1} - \frac{dh_z}{dr} - j_{\theta_0} = 0 \qquad (64)$$

$$\left.\begin{aligned} i\gamma e_\theta + i\omega\mu h_r &= 0 \\ \tfrac{1}{r}\tfrac{d}{dr}(r e_\theta) + i\omega\mu h_z &= 0 \end{aligned}\right\} \qquad (65)$$

$$\dot{\zeta}_\theta = \sigma e_\theta \qquad (66)$$

$$\nabla^2 u_\theta - \tfrac{1}{r^2} u_\theta + \frac{\rho\omega^2}{G} u_\theta = 0 \qquad (67)$$

Hence it is seen that the equations are not coupled in this case. In particular, equation (67) yields a purely elastic wave in a hollow cylinder, a problem which has been solved by Gazis[11, 12]. This case in itself hence is of no further interest. However, it will be instructive in the next case if the equation governing the electromagnetic wave is obtained. This is done exactly as before by elimination of the other variables and the equation is:

$$\mathcal{L} h_r - i\sigma\omega\mu h_r = 0 \qquad (68)$$

which has the solution

$$h_r = A_1 I_1(\lambda_2 r) + B_1 K_1(\lambda_2 r) \qquad (69)$$

where

$$\lambda_2^2 = \gamma^2 + i\sigma\omega\mu \qquad (70)$$

The boundary condition as given by equation (27) is:

$$h_r \Big|_{\substack{r=a \\ r=b}} = 0 \qquad (71)$$

This is quite similar to the problem solved by Gazis except this involves modified Bessel functions with complex arguments. In his

analysis of the simpler problem Gazis was forced to resort to the use of a digital computer, hence this case will not be pursued further, especially in view of the uncoupling of the elastic wave.

II. Case IV: Axial Electric Field

The configuration for this case is the same as that shown in Fig. 4 except an axial electric field is applied. This field is given by:

$$\vec{E}_0 = E_z \hat{i}_z \qquad (72)$$

and induces the following magnetic field within the conductor.

$$(H_\theta)_E = \frac{\sigma E_z}{2}(1 - \beta^2/1)$$

Hence the total magnetic field is given by

$$\vec{H}_0 = \left[\frac{\sigma E_z}{2}(1 - \beta^2/1) + \tfrac{1}{1} H_\theta\right] \hat{i}_\theta \qquad (73)$$

If these fields are introduced into the governing equations they become

$$\nabla \times \vec{h} = \vec{j} \qquad (74)$$

$$\nabla \times \vec{e} + \mu \frac{\partial \vec{h}}{\partial t} = 0 \qquad (75)$$

$$\vec{j} = \sigma \vec{e} \qquad (76)$$

$$G \nabla^2 \vec{u}_\theta - \rho \frac{\partial^2 \vec{u}_\theta}{\partial t^2} + \mu\{-[\tilde{H}_\theta j_z + \sigma E_z h_\theta] \hat{i}_1 + \sigma E_z h_1 \hat{i}_\theta + \tilde{H}_\theta j_1 \hat{i}_z\} = \mu \sigma E_z \tilde{H}_\theta \qquad (77)$$

where

$$\tilde{H}_\theta = \left[\frac{\sigma E_z}{2}(1 - \beta^2/1) + \tfrac{1}{1} H_\theta\right] \qquad (78)$$

The term on the left hand side of equation (77) represents a steady state stress due to the combined effects of the electromagnetic fields. Since the problem is linear it may be ignored in seeking the time dependent solution. Doing so, the equations are written in component form as:

$$\left.\begin{aligned} & i\gamma h_\theta - j_r = 0 \\ & -i\gamma h_r - \frac{\partial h_z}{\partial r} - j_\theta = 0 \\ & \tfrac{1}{r}\frac{\partial}{\partial r}(r h_\theta) - j_z = 0 \end{aligned}\right\} \qquad (74)$$

$$\left.\begin{aligned} & i\gamma e_\theta + i\omega\mu h_r = 0 \\ & -i\gamma e_r - \frac{\partial e_z}{\partial r} + i\omega\mu h_\theta = 0 \\ & \tfrac{1}{r}\frac{\partial}{\partial r}(r e_\theta) + i\omega\mu h_z = 0 \end{aligned}\right\} \qquad (75)$$

$$\vec{j} = \sigma\vec{e} \qquad (76)$$

$$\left.\begin{aligned} & \tilde{H}_\theta j_z + \sigma E_z h_\theta = 0 \\ & G[\nabla^2 u_\theta - \tfrac{1}{r^2}u_\theta] + \rho\omega^2 u_\theta + \mu\sigma E_z h_r = 0 \\ & \tilde{H}_\theta j_r = 0 \end{aligned}\right\} \qquad (77')$$

The last of equation (77') implies $j_r = 0$, which leads as before to the following set of conditions:

$u_r = 0$	h_r	$j_r = 0$	$e_r = 0$
u_θ	$h_\theta = 0$	$j_\theta =$	e_θ
$u_z = 0$	h_z	$j_z = 0$	$e_z = 0$

The remaining equations are:

$$i\gamma h_1 + \frac{dh_z}{dr} + j_\theta = 0 \qquad (74)$$

$$\left.\begin{aligned} i\gamma e_\theta + i\omega\mu h_1 &= 0 \\ \tfrac{1}{r}\frac{d}{dr}(r e_\theta) + i\omega\mu h_z &= 0 \end{aligned}\right\} \qquad (75)$$

$$j_\theta = \sigma e_\theta \qquad (76)$$

$$G[\nabla^2 u_\theta - \tfrac{1}{r^2} u_\theta] + \rho\omega^2 u_\theta + \mu\sigma E_z h_1 = 0 \qquad (77')$$

Note that equations (74) through (76) are identical to the corresponding ones of the previous case, hence the equations of motion may be written down immediately.

$$L h_1 - i\tfrac{1}{c^2} h_1 = 0 \qquad (78)$$

$$L u_\theta + (\omega/v_s)^2 + \frac{\mu\sigma E_z}{G} h_1 = 0 \qquad (79)$$

Equation (78) is identical to the previous case and may be solved directly. The solution as given by equation (69) is

$$h_1 = A_1 I_1(\lambda_z r) + B_1 K_1(\lambda_z r) \qquad (69)$$

with

$$\lambda_z^2 = \gamma^2 + i\tfrac{1}{c^2}$$

The coupling term of equation (79) is now determined and this equation may also be solved. The homogeneous solution is given by equation (48) as

$$(u_\theta)_0 = A J_1(\lambda,\pi) + B Y_1(\lambda,\pi) \qquad (78)$$

with

$$\lambda_1^2 = \gamma^2 - (\omega/v_s)^2$$

The particular solution is obtained by means of the general expressions for a particular solution of an ordinary differential equation, i.e.

$$(u_\theta)_p = v_1(\lambda,\pi) J_1(\lambda,\pi) + v_2(\lambda,\pi) Y_1(\lambda,\pi) \qquad (80)$$

where if $\lambda_1 \pi = x$

and $\lambda_2 \pi = y$

the variable coefficients are given after some algebra by

$$\frac{dv_1}{dx} = -\frac{\pi x}{2} Y_1(x)[P I_1(y) + Q K_1(y)] \qquad (81)$$

$$\frac{dv_2}{dx} = \frac{\pi x}{2} J_1(x)[P I_1(y) + Q K_1(y)] \qquad (82)$$

with

$$P = -\frac{\mu \sigma E_z}{G} A$$

$$Q = -\frac{\mu \sigma E_z}{G} B$$

To obtain the complete solution integrals of the following form must be evaluated.

$$I = \int_0^{\pi} s\, J_1(s)\, I_1(\phi_1 s)\, ds$$

where

$$\phi_1 = \lambda_2/\lambda_1$$

This indefinite integral involving a product of Bessel functions with complex arguments is difficult to evaluate. In fact, the best that may conveniently be done is to expand one of the Bessel functions in an appropriate asymptotic expansion and integrate term by term. If this task is accomplished the boundary condition must be applied to obtain the numerical values of λ_1 and λ_2. Recalling that the task of evaluating λ_1, for the homogeneous case, which corresponds to case III, required machine computation the full difficulty of this problem will be recognized. It is therefore deemed an unwise course of action to pursue this problem in this manner any further. An alternative method to this general type of problem is suggested by Miles. [7] He studied the radial mode of vibration of a hollow rod as a shallow shell. Applying membrane theory he obtained a solution; however, even with this approach he was forced to restrict the problem to one in which the hollow rod had zero hoop stress.

SECTION D: CONCLUSIONS

The results of this investigation may be summarized as follows:

Case I. Solid rod with axial electric and magnetic fields.

It was found that a pure torsional wave that is coupled to the electromagnetic fields will not propagate under these conditions.

Case II. Solid rod with axial magnetic field only.

A pure torsional wave was found that will propagate over a restricted range of frequencies. Below this range the waves uncouple and the pure elastic torsional wave results. Above this range higher modes are introduced which are highly damped.

Case III. Hollow rod with tangential magnetic field only.

The elastic wave and magnetic effects are completely uncoupled.

Case IV. Hollow rod with tangential magnetic field and axial electric field.

The equations of motion are obtained and the secondary coupling due to the magnetic field induced by the axial electric field is noted. The coupling in this case is not thoroughly investigated due to mathematical difficulties which arise.

In general the effect of the magnetic field on a torsional wave is found to be quite small. Case II was found to be the most interesting from the viewpoint of a possible configuration for experiment investigation. However, if an axial displacement were permitted as well as the pure torsional displacement, Case I would become of equal importance.

REFERENCES

1. L. Knopoff: The interaction between wave motions and a magnetic field in electrical conductors, Jour. Geophys. Res., 60, 441-456, (1955).

2. P. Chadwick: Elastic wave propagation in a magnetic field, IX. Congres International de Mecanique Appliquee, Brussels, (1956).

3. S. Kaliski and J. Petykiewicz: Dynamical equation of motion and solving function for elastic and inelastic anisotropic bodies in the magnetic field, Proceedings of Vibration Problems, Vol. 1, No. 2, Warsaw (1959).

4. S. Kaliski: Solution of the equation of motion in a magnetic field for an isotropic body in an infinite space assuming perfect electric conductivity, Proceedings of Vibration Problems, Vol. 1, No. 3, (1959).

5. S. Kaliski and D. Rogula: Rayleigh waves in a magnetic field in the case of a perfect conductor, Proceedings of Vibration Problems, Vol. 1, No. 5, (1960).

6. I. C. Percival: Waves in a conducting sheet situated in a strong magnetic field, Proc. Phys. Soc., 76, 329, (1960).

7. J. W. Miles: Waves on a thin conducting shell in a magnetic field, Proc. Phys. Soc., 79, 399-402, (1962).

8. J. W. Dunkin and A. C. Eringen: On the propagation of waves in an electromagnetic elastic solid, Technical Report No. 18, School of Aeronautical and Engineering Sciences, Purdue University, May, (1961), (ASTIA No. AD 257-476).

9. R. A. Willett: An experiment in magnetoelasticity, Thesis, UCLA, (1957).

10. G. N. Watson: Theory of Bessel Functions, Second Edition, Cambridge University Press, (1952).

11. D. C. Gazis: Exact analysis of the plane-strain vibrations of thick-walled hollow cylinders, The Journal of the Acoustical Society of America, Vol. 30, No. 8, Aug., (1958).

12. D. C. Gazis: Three-dimensional investigation of the propagation of waves in hollow circular cylinders, I Analytical foundation, II Numerical results, The Journal of the Acoustical Society of America, Vol. 31, No. 5, May, (1959).

13. E. Jaknke and F. Emde: Tables of Functions, Dover, (1945).

14. J. A. Stratton: Electromagnetic Theory, McGraw-Hill Book Co., Inc., New York, N. Y., (1941).